

NASA
TP
1141
c.1

NASA Technical Paper 1141

LOAN COPY:
AFWL TECHNIC
KIRTLAND AF

TECH LIBRARY KAFB, NM
0134502

The Optical Absorption
of Triatomic Carbon C₃
for the Wavelength Range

260 to 560 nm

Jim J. Jones

MARCH 1978

NASA



Received by
AF Space
Lab Kirtland



0134502

NASA Technical Paper 1141

The Optical Absorption of Triatomic Carbon C₃ for the Wavelength Range 260 to 560 nm

Jim J. Jones
Langley Research Center
Hampton, Virginia



National Aeronautics
and Space Administration

**Scientific and Technical
Information Office**

1978

SUMMARY

The spectral absorption properties of C_3 have been measured in a shock tube containing a test-gas mixture of acetylene diluted with argon. The absorption of a pulsed xenon light source was measured by means of eight photomultiplier channels to a spectrograph and an accompanying drum camera. The postshock test-gas temperature and pressure were varied over the ranges 3240 to 4300 K and 37 to 229 kPa, respectively.

The results showed appreciable absorption by C_3 for the wavelength range 300 to 540 nm. The various reported measurements of the heat of formation of C_3 which are available in the open literature have been reviewed, and a value of 198 kcal/mol is recommended. This value, along with best available values for other species, was used to calculate the number density of C_3 for the conditions of the present experiments in order to compute absorption cross section or electronic oscillator strength. The computed electronic oscillator strength varied from a high of 0.062 at 3300 K to a low of 0.036 at 3900 K.

INTRODUCTION

Entry into the atmospheres of the outer planets is accompanied by large radiative heating of the entry probe forebody. To some degree, this thermal radiation is blocked (absorbed) by the cooler gases being evolved from the ablative heat shield. For example, reference 1 shows that the ablation gases emitted from a phenolic-carbon heat shield absorb about half the incident radiant energy for an entry into the atmosphere of the planet Jupiter. Although the calculation method used in reference 1 is the best available estimate of the absorption effects of the ablator gases, its accuracy is hampered by the limited knowledge of the absorption properties of the various gas species present. Under the assumption of thermochemical equilibrium, the calculations predict that a significant fraction of the ablator gas will be composed of such molecules as C_3 , C_4 , C_5 , C_2H , and C_3H , for which little or no information is available on spectral absorption properties.

Reference 1 indicates that C_3 is the dominant species near the ablator wall, with a mole fraction exceeding 0.5 for some cases. Thus, an accurate determination of its spectral absorption cross section will greatly benefit the radiant transfer calculations. The present study examines the absorption by triatomic carbon C_3 in the spectral range 260 to 560 nm.

The most prominent spectral feature of C_3 is a continuum-band system in the vicinity of 400 nm. Frequently referred to as the " $\lambda 4050 \text{ \AA}$ bands" (ref. 2), and first observed in cometary spectra, this line group has been shown (ref. 3) to be due to a ground-state-connected electronic transition in the C_3 molecule. Only a few lines are observed at cryogenic temperatures (e.g., refs. 4 to 7), but at elevated temperatures, a strong apparent continuum dominates this spectral region (ref. 2). This apparent continuum was shown

by Brewer and Engelke (ref. 8) to be due to the same bound states as the observed lines and, therefore, not a true continuum but a "pseudocontinuum" of very closely spaced rotational lines of the electronic transition. Reference 8 includes an absorption measurement in saturated carbon vapor at a temperature of 3200 K. The estimate of C_3 number density given in reference 8 was used in reference 9 to convert these data to spectral cross section. These appear to be the only quantitative data on C_3 absorption at high temperatures that are available in the open literature.

In the present study, the species C_3 was produced by shock heating an acetylene-argon test-gas mixture in a shock tube. The calculated temperature behind the incident shock wave, based on shock velocity measurements, ranged from about 3240 to 4300 K. The postshock pressure varied from 37 to 229 kPa. The postshock test gas was viewed in absorption by means of a high-pressure xenon pulsed light source. The number density was calculated by using the measured shock velocity and assuming thermochemical equilibrium. From the measured absorption and the calculated number density, the spectral absorption cross section was calculated for the spectral range 260 to 560 nm. The variation of this spectral absorption cross section with temperature is obtained for the temperature range of the experiments.

SYMBOLS

Values are given in SI Units except for heat content, which is given in calories (1 cal = 4.184 J). Following common practice, the abbreviation eu is used for entropy units of calories per degree kelvin per mole.

a	radius of carbon particulates, nm
$a_0, a_1,$ } a_2, a_3	coefficients in curve fit of absorption cross section as a function of temperature (eq. (8))
c	velocity of light, cm/sec
c_p	specific heat at constant pressure, cal/mol-K
D	film density
E	film exposure, arbitrary units
e	charge of an electron, C
$e(t)$	time-dependent emission of the test gas as measured by a spectrograph-channel photomultiplier tube
$F(t)$	time-dependent absorption defined by equation (1)
$F'(t)$	absorption parameter corrected for gas emission, as defined by equation (2)
f	focal length, m

f_e	electronic oscillator strength
G_T	Gibbs free energy at temperature T , cal/mol
h	static enthalpy, cal/mol
I	light intensity, arbitrary units
I_o	unattenuated light intensity, arbitrary units
I_s	light intensity after passing through test gas with path length s , arbitrary units
K_λ, K_ω	extinction coefficient at wavelength λ or wave number ω , cm^{-1}
m	mass of electron, kg
\bar{m}	mass of carbon particulates per unit flow volume, kg/m^3
N	number density, cm^{-3}
N_1, N_2	real and imaginary components, respectively, of refractive index of carbon
p	pressure, Pa
p_λ	Rayleigh factor
R	universal gas constant, $8314 \text{ J}/\text{kmol}\cdot\text{K}$ ($1.987 \text{ cal}/\text{mol}\cdot\text{K}$)
S_T	entropy at temperature T , cal/mol-K
$S(t)$	time-dependent photomultiplier signal
s	optical path length through test gas, cm
T	temperature, K
T_2	calculated equilibrium test-gas temperature immediately behind incident shock wave, K
t	time, sec
V_s	velocity of incident shock wave, km/sec
x	distance along shock tube measured from diaphragm, m
γ	slope of linear portion of film sensitivity curve (eq. (3))
$\bar{\gamma}$	mean isentropic exponent for test gas

ΔH_T° heat of formation at pressure of 1 atm (101 kPa) and temperature T , kcal/mol
 λ wavelength, nm
 ρ_c density of graphite, kg/m³
 $\sigma_\lambda, \sigma_\omega$ absorption cross section at wavelength λ or wave number ω , cm²
 ω wave number, cm⁻¹

Subscripts:

abs	absorption
p	particles
sca	scattering
0	prerun condition for light signal
1	condition before shock arrival
2	condition behind incident shock
50	calculated conditions 50 μ sec after shock passage

EXPERIMENTAL APPARATUS

Shock Tube

The shock tube used in the present investigation is the same facility described in reference 10. It is an all-stainless-steel tube 15.2 cm in internal diameter with a driven tube approximately 15.4 m long. The electric arc electrode assembly was removed from the driver chamber and a driver extension section was added to make a driver chamber length of 2.44 m. The boundary-layer splitter-plate assembly in the test section was not used, since in the present study the postshock flow Mach numbers were less than 2, and preliminary tests indicated that the splitter-plate assembly sometimes choked the flow. Thus, the test-section windows were mounted flush with the tube walls.

Helium was used as the driver gas for all runs. After preliminary evacuation, helium was injected into the driver chamber until the diaphragm ruptured. Diaphragms were stainless steel with the conventional grooves machined in a cross pattern to cause the diaphragm to open in the usual four-petal configuration.

The driven chamber was initially evacuated to a pressure of approximately 0.03 Pa by using a diffusion pump and a liquid-nitrogen-cooled trap. The test gas was injected into the chamber approximately 3 to 5 minutes prior to the run. The increase in chamber pressure due to outgassing and leakage was approximately

0.07 Pa/min. Since the initial test-gas pressure was 700 Pa or greater, the ratio of air and water vapor to test gas was believed to be 6×10^{-4} or less for all runs.

Optical Instrumentation

A schematic drawing of the optical arrangement and shock tube is shown in figure 1. The light source was a high-pressure xenon lamp which was pulsed by the discharge of a capacitor-inductor transmission line to produce a nearly constant light intensity for about 1 msec. This pulse was initiated by the passage of the shock wave at a station upstream of the test section, so that the light pulse was initiated 200 to 300 μ sec prior to the arrival of the shock wave at the window location. Quartz lenses were used to form an image of the lamp on a small orifice 1.8 mm in diameter and then to form a collimated beam using the image at the orifice as the apparent source. Another lens focused this beam on the spectrograph entrance slit. Field stops 1 cm in diameter were used at the window locations and along the collimated beam path to reduce stray light and define the geometry of the optical path.

The spectrograph used was a Czerny-Turner mount with a nominal aperture of f/6.3. Internal masks were used to insure that the spectrograph was filled with light. These masks limited the spectrograph to approximately f/8. The spectrograph was modified by inserting a front-surface mirror which reflected approximately 80 percent of the light into a rotating-mirror camera which had been adapted to the spectrograph. The remaining 20 percent of the light passed over the top of the mirror and fell on the focal plane. Eight light pipes were mounted in a group with their entrance faces at the focal plane. Each light pipe led to a photomultiplier tube. When used in the ultraviolet range, the entrance faces of the light pipes were coated with sodium salicyclate. The effective width of the light pipes ranged from 1.1 to 1.9 mm. Therefore, the effective band pass was 4.3 to 7.7 nm and 2.1 to 3.8 nm for the two gratings used in the investigations. The gratings used were a 300 line/mm grating blazed at 500 nm and a 600 line/mm grating blazed at 300 nm. The approximate values of linear dispersion at the focal plane were 41.0 nm/cm for the 300 line/mm grating and 20.2 nm/cm for the 600 line/mm grating.

The photomultipliers were used with load resistors that limited output current to less than 1 mA. The linearity of each photomultiplier tube was checked with neutral-density filters. An example of the linearity check is shown in figure 2 for one channel. On each channel, ballast capacitors paralleled each of the last two resistors of the dynode chain so as to maintain nearly constant dynode voltages for extended signal periods.

The drum camera was a commercially manufactured device which was modified to adapt to the spectrograph. It used an air-driven turbine to turn the drum 318 ± 5 rps. The length of film (internal circumference of the drum) was 31.88 cm, and therefore the film speed was 10.1 ± 0.1 cm/msec. Since the effective slit height at the film was approximately 1.5 mm, the time resolution on the film was no better than 15 μ sec.

Velocity-Pressure Instrumentation

The distances from the primary diaphragm to the centers of the instrumentation ports are shown in table I. A thin-film resistance thermometer was installed in station 1 to detect the passage of the shock wave. The output signal from this gage was used to initiate both the system of time-interval meters which measured the shock transit times and the time-delay generators which triggered the oscilloscopes.

The remaining instrumentation ports had either thin-film gages, light pipes leading to photomultipliers, or quartz pressure transducers mounted as indicated in table I. The thin-film gages were used because they gave low-noise, rapid-rising signals which were easily amplified for use as trigger signals. The photomultipliers merely gave an indication of the approximate test time. The pressure transducers showed the steadiness of the test-gas slug. Examples of the oscillograms from a photomultiplier and a pressure transducer are shown in figure 3.

The shock velocity was determined from the measurements of time-interval meters. The amplified signal from the instrumentation mounted at each station was used to stop a time-interval meter. The start gate for all the time-interval meters was provided by the thin-film gage at station 1. An example of the calculated average velocity between successive stations is shown in figure 4.

The shock attenuation ranged from 5 to 20 $\frac{\text{m/sec}}{\text{m}}$ depending on the pressure level. The velocity which was used to reduce the data was the final velocity at the test section.

Test Gas

The test gas was purchased already mixed and certified by the supplier to be 2.99 percent C_2H_2 , 97.01 percent argon by volume. A few runs were made as a check with a 1.97-percent C_2H_2 , 98.03-percent argon mixture. Twice during the test program, a sample of the test gas was analyzed by gas chromatography to insure that the mixture remained uniform.

Test Procedure

It was found that if the lamp had not been fired for several hours, it was necessary to fire it several times in order to insure reproducible light pulses. After these warmup firings, the lamp regularly reproduced an identical pulse within ± 5 percent. When the lamp had been fired sufficiently to insure good repeatability, a prerun shot was recorded from the eight photomultipliers connected to the spectrograph light pipes. These records were regarded as the unabsorbed intensity as a function of time for each channel. The capacitor bank which fired the lamp was charged to 355 V, as read on a digital voltmeter, for the prerun record.

As mentioned previously, the driven chamber was evacuated to about 0.03 Pa prior to each run. The driver chamber was evacuated to about 1.5 Pa by using a mechanical pump only. After the test gas was injected into the driven tube, the lamp supply capacitors were charged to approximately 365 V. Since the charge slowly leaked off the capacitors, the succeeding run operation steps were paced in an attempt to synchronize the diaphragm rupture with a capacitor voltmeter reading of 355 V. This result was accomplished within ± 2 V for nearly all runs.

Following each run, the shock-tube windows were cleaned, since postrun lamp firings showed that the intensity was reduced by 10 percent or so as a result of deposits on the windows. The entire shock-tube interior was cleaned periodically (approximately every 20 runs) with ethyl alcohol.

DATA REDUCTION PROCEDURES

Spectrograph Channels

A sample record from a spectrograph channel is shown in figure 5. Figure 5(a) shows the prerun record of the light pulse, and figure 5(b) shows the oscillogram taken during the run. The arrival of the shock wave is clearly indicated by the sudden drop in photomultiplier signal level. Figure 5(c) shows the record after being digitized, along with the digitized prerun record for the same channel. Figure 5(d) presents the fraction of light absorbed

$$F(t) = \frac{S_0(t) - S(t)}{S_0(t)} \quad (1)$$

where $S(t)$ and $S_0(t)$ are the time-varying values of the photomultiplier signal for the run and prerun, respectively. For these traces, time equal to zero corresponds to the start of the light pulse.

The parameter $F(t)$ was plotted for each channel of each run by a programmable calculator with the digitized oscillograms as input data. Typically, the value of $F(t)$ increased moderately with time after shock passage, most likely because of the growing wall boundary layer. Many runs showed that the parameter $F(t)$ took 40 μ sec or so to reach a plateau value, suggesting that the chemical relaxation rate took approximately this long to adjust to the postshock condition.

The light received by the spectrograph included the emission from the gas as well as the (partially absorbed) emission from the lamp. In order to determine the contribution from gas emission, runs were made with the lamp turned off. For some runs, a light chopper was employed so that the absorption and emission could be determined on the same run. The field stops in the light path attempted to insure that the volume of gas contributing to the emission was essentially the same as that for which the absorption was determined.

The emitted light was expressed as a fraction of the prerun lamp signal S_0 , and this quantity was used to correct the absorption parameter $F(t)$. If

the corrected absorption is denoted as $F'(t)$ and the emission as $e(t)$, the following expression results:

$$F'(t) = \frac{S_0(t) - [S(t) - e(t)]}{S_0(t)} = F(t) + \frac{e(t)}{S_0(t)} \quad (2)$$

For most run conditions, the emission term was immeasurably small. For the highest temperature runs, the emission term grew as large as $\frac{e(t)}{S_0(t)} = 0.1$ and represented a correction to the value of $F(t)$ of the order of 30 percent. A few runs were made in pure argon test gas to insure that the emission and absorption from the carrier gas were negligible.

Drum Camera Film

A sample of the film obtained from the drum camera is shown in figure 6(a). The prominent features of the absorption are an apparent continuum and a few bands. All the bands that were observed over the entire wavelength range of the study belong either to C_2 or the violet system of CN. This latter system is so strong that only a small contamination of air in the test-gas mixture causes it to appear.

Figure 6(b) shows a microdensitometer tracing of the film for the same run as that of figure 6(a). Two traces are shown, one taken at a time just before shock arrival and the other taken about 100 μ sec after shock arrival. The difference between the traces is a measure of the absorption.

The film yields so much more spectral detail than the light pipe channels that an attempt was made to use the densitometer traces quantitatively. The following procedure discusses how this was done. It must be emphasized, however, that only limited confidence can be attached to the quantitative film density results, because of the many pitfalls associated with using film quantitatively and the approximate procedure used in the present study.

Twice during the investigation, sensitometer samples were made on film samples and these were developed in the same manner as the test films. The sensitometer samples were then run on the microdensitometer and the specular density of the film was plotted against the logarithm of the exposure, as shown in figure 7. The linear portion of this curve showed a slope of approximately $\gamma = 0.9$. The film density D was thus assumed to be related to exposure by

$$D_1 - D_2 = \gamma [\log_{10} (E_1) - \log_{10} (E_2)] \quad (3)$$

where the subscripts 1 and 2 indicate times just before and just after shock arrival, respectively. Exposure is defined as the product of the light intensity and time; therefore, equation (3) may be rewritten

$$\frac{E_1}{E_2} = \frac{I_1 t}{I_2 t} = 10^{(D_1 - D_2)/\gamma} \quad (4)$$

Since the exposure time is the same for each element on the test film, equation (4) yields the ratio of light intensity before shock arrival to that after the shock as a function of density difference on film. This ratio was then used to determine the wavelength-dependent extinction coefficient K_λ . As noted previously, the values of extinction coefficient determined from the film must be viewed with great caution. However, as is shown subsequently, they show quite good repeatability and are in essential agreement with the data obtained from the light pipe-photomultiplier channels. The two most daring assumptions in the procedure just described appear to be

(1) The determination of the slope γ was made by using the xenon flash lamp in the sensitometer, and these "white" light data were then assumed to apply for all wavelengths throughout the spectral range of the investigation and for all film exposures, even though at low film density, the slope was distinctly lower.

(2) The same calibration data were assumed to apply for all runs; thus any differences in film development from run to run were ignored.

Absorption Cross Section

The extinction coefficient K_λ is defined by the relation

$$dI = -K_\lambda(s)I ds \quad (5)$$

(See ref. 11 for a review of fundamentals in absorbing media.) If the absorbing medium has uniform absorbing and scattering properties along the length of the light path s , equation (5) may be integrated from 0 to s to yield

$$K_\lambda = \frac{\ln \frac{I_0}{I_s}}{s} \quad (6)$$

Here, I_0 and I_s denote, respectively, the intensity as the light beam enters and leaves the absorbing medium of length s .

In the present study, scattering effects were ignored and the absorption coefficient was assumed identical with the extinction coefficient. Solid particles, if present, would be expected to be a significant scattering agent. For this reason, the present test conditions avoid the lower temperature range, where solid carbon particles might be expected to be present. In "Results and Discussion," tests are described which support the conclusion that the present experiments are not significantly affected by solid particle scattering.

An absorption cross section may be defined as

$$\sigma_\lambda \equiv \frac{K_\lambda}{N_{C_3}} \quad (7)$$

Use of the absorption cross section to define the absorption properties of a gas accounts for the dependence of absorption coefficient on gas density by assuming a linear variation with the number of molecules available to absorb. Reduction and use of the present data therefore require that the number density of C_3 molecules be determined.

For the present tests, the number density of C_3 molecules was determined by a free-energy-minimization calculation assuming thermochemical equilibrium in the test region behind the shock wave. The chemical equilibrium computer program ACE of reference 12 was used for this calculation; the thermodynamic state properties ahead of the shock wave and the shock velocity for each run were required inputs to the program. The program also requires a value for heat of formation and a definition of the temperature-dependent thermodynamic variables for each gas species which is to be considered in the final mixture. This requirement creates a problem in that the heat of formation of C_3 has not been determined as accurately as is desirable. Measurements of the heat of formation of C_3 range from $\Delta H_0 = 188$ kcal/mol (ref. 13) to as high as $\Delta H_{298} = 212$ kcal/mol (ref. 14). This spread in heat of formation, together with the uncertainty in thermal properties, produced an unacceptably large difference in the calculated number density of C_3 . Consequently, a review of the various measurements of the heat of formation and thermal property calculations of C_3 was included in the present study and is reported in the appendix. The thermal property calculations of Lee and Sanborn (ref. 15) and a heat of formation $\Delta H_0 = 198$ kcal/mol were selected and used in the ACE program for computing the C_3 number density.

Varying Stream Properties

As was stated previously, the absorption parameter $F'(t)$ usually increased moderately with time after shock passage. Three possible causes of this time variation of absorption are suggested: (1) the flow might not be in chemical equilibrium; (2) the free-stream properties vary as a result of the displacement effects of the boundary layer; and (3) the boundary layer, which grows with distance behind the shock wave, absorbs more per unit optical path length than does the inviscid flow. In this section, these possible causes are examined in turn in an effort to evaluate their effects on the present data.

Thermochemical equilibrium.- Since rate constants for the important reactions are not well known, a finite-rate calculation of the reaction process would not be reliable. However, several facets of the present data suggest that chemical equilibrium was essentially obtained in about 40 μ sec after shock passage. (It might be noted that the residence time of the particles was about 4 times greater than the observation time. Thus, at an observation time of 40 μ sec, the observed gas particles passed through the shock wave approximately

160 μ sec earlier.) These various facets that suggest chemical equilibrium for the present test conditions are now briefly enumerated:

(1) The photomultiplier tubes used to detect shock wave and interface passage typically displayed signals which rose to a level in 20 to 40 μ sec. Thereafter, the signal level either decayed somewhat (as in the example in fig. 3(a)) or remained essentially constant. Since these light signals were not filtered spectrally, they contained contributions from all emitters within the spectral range of the detector (possibly including impurities) and would be expected to be quite sensitive to temperature variations. Thus, the relative flatness of the signal would seem to imply only small temperature variation with time.

(2) On runs in which the emission was measured with the spectrograph (i.e., the absorption lamp source was not used), the emission at each wavelength rose to a plateau in about 20 μ sec after shock passage and then remained remarkably constant for the remainder of the test time. This emission was assumed to be due to C₃ and therefore implied constant number density and temperature of the C₃ species.

(3) Timewise surveys of the drum camera films at the wavelengths of the band heads of the C₂ Swan band system were also very constant with time. Thus, the absorption due to C₂ was essentially time invariant. Also, the measured absorption coefficient was in fairly good agreement with that predicted by reference 16.

(4) The results of runs for a test-gas mixture of 2 percent acetylene in argon were in good agreement with the results for a 3-percent acetylene mixture. Also, no significant trends with pressure level were observed.

Effects of varying free-stream properties. - Mirels has shown (ref. 17) that the free-stream flow properties vary with distance behind the shock wave because the growing wall boundary layer changes the effective cross-sectional area of the inviscid flow. Reference 17 presents relationships for calculating the varying flow properties, for either wholly laminar or wholly turbulent boundary-layer growth, based on the assumption of an isentropic process in the postshock inviscid flow. For the present data, a turbulent boundary layer has been assumed because of the Reynolds number range of the test conditions. This assumption appears justified, since the measured test times were in good agreement with those calculated by the method of reference 18 for a turbulent boundary layer.

Four runs were selected as approximately bounding the pressure-temperature range of the present tests. An isentropic exponent based on the equilibrium mole fractions of the major species was calculated for each of these runs. The mean value of this isentropic exponent γ was 1.654, and this value was used for all runs to compute the isentropic compression of the shocked gas, starting with the postshock equilibrium conditions. Figure 8 shows the computed temperature variation at the test location for the four sample runs. It may be seen that the temperature variation T/T₂ is very similar for all four runs; therefore, for all runs of the test program, the time variation of the postshock temperature was modelled as

$$T/T_2 = 1 + 0.0066(t \times 10^6)^{0.3}$$

This relation is also shown in figure 8. The pressure variation was then found by the isentropic relation $p \propto T^{\bar{\gamma}/(\bar{\gamma}-1)}$.

In a similar manner, the variation of the mole fraction of C_3 was curve fit for the present test range as a function of pressure and temperature. This permitted determination of the time-varying number density as a perturbation of the value calculated immediately behind the shock wave.

Figures 9(a), 9(b), and 9(c) show examples of the effect of applying the time-varying number density to the absorption data. As illustrated by figure 9, this calculation method was not uniformly successful in accounting for the time variation of the absorption. In fact, for the highest temperature conditions, the absorption cross section varies more with time than does the absorption factor $F'(t)$. It seems apparent that correction for the variation of free-stream properties will not by itself yield a time-invariant absorption cross section.

Boundary-layer absorption.— No analysis of the absorption within the boundary layer was attempted in the present study, and for the data reduction a constant value for the absorption path length equal to the tube internal diameter was used. This would imply that the number density of C_3 per unit path length in the boundary layer was the same as that in the inviscid stream. Such a case would not usually exist, of course, and it appears likely that the variation of the absorption with time is, to a large extent, the result of varying C_3 number density in the viscous region. Therefore, this effect is minimized by evaluating the absorption at the shortest possible time after shock passage.

Accordingly, the present data were evaluated 50 μ sec after shock passage. The temperature and pressure at this time, designated T_{50} and p_{50} , were 2 percent and 5.5 percent, respectively, greater than the postshock values. The number densities of C_3 used for the present data were obtained by first calculating the number density immediately behind the shock wave with the equilibrium chemistry program ACE and then using curve-fit relations as a perturbation on this value to account for the change in composition as the pressure and temperature rose from the values p_2 and T_2 to p_{50} and T_{50} .

Spectrum Identification

Since a number of gas species are expected to be present in the test-gas sample, the portion of the total absorption spectrum which is attributable to C_3 must be determined. Figure 10 shows the mole fractions of the principal species which are predicted to be present behind the incident shock wave as a function of shock velocity. For this example, the initial pressure was held constant at 1.72 kPa, which is typical for the present data. Argon, which of course is the most abundant species, has been omitted from figure 10. The figure shows other important species present to be H, H_2 , C, C_2 , C_3 , C_2H , and C_3H . Of these, the first four have well-identified spectra which may be recognized

and subtracted out if they appear in the present data. The spectra of the latter two, C₂H and C₃H, are not known; therefore, any contribution they may make to the present absorption data could go unrecognized. However, both species have distinctly different variations with temperature than C₃, and thus a comparison of high-temperature and low-temperature absorption spectra should be helpful in identifying any contribution these species may make. In reference 19, a spectrum for C₂H was synthesized by analogy to similar molecules. This synthesized spectrum does not include any transitions in the wavelength range of the present data.

RESULTS AND DISCUSSION

The basic experimental results are presented in table II for the 3-percent acetylene mixture and table III for the 2-percent mixture. The shock velocity and postshock temperature and pressure T₅₀ and p₅₀ are tabulated as well as the absorption cross sections obtained from the eight spectrograph channels. For each channel, the central wavelength for each light pipe is noted, and the corresponding cross-section measurement is given directly below. For certain wavelength settings of the grating, some "stray light" was noted on channels 1 and 2. When this occurred, data from these channels were not included in the tables. Here the term "stray light" refers to light emanating from the pulsed light source, but of the wrong wavelength for that particular channel. At each grating position, a check for stray light was made by means of a series of band-pass filters inserted in the light beam at the entrance slit to the spectrograph.

Constant-Temperature Survey

Figure 11 presents the absorption cross section for seven runs in which the postshock test state was repeated as closely as possible. The temperature was 3723 ± 47 K for these runs, which are runs 1 to 7 in table II. Between these runs, the grating position was changed to move the spectral setting of the channels by about 35 nm. Thus, a complete spectral survey was obtained at nearly constant test conditions. Figure 11 shows the photomultiplier data for the seven runs as square symbols. For two of these runs, the data from the densitometer readings of the film are shown as solid lines. The data from the film are seen to be in good agreement quantitatively with the photomultiplier data, particularly near the absorption peak, and confirm that the absorption profile is essentially smoothly varying, with the only distinctive features being due to the contaminant CN and the band heads of the C₂ Swan system.

In order to compare the present results with those of Brewer and Engelke (ref. 8), another survey was made at lower temperature. Figure 12 shows this survey, for which the mean temperature was 3240 K, and the results of reference 8, for which the mean temperature was 3200 K (solid curve). To obtain this latter curve, the absorption data shown in figure 1 of reference 8 were used, and the number density of C₃ was computed by using the thermal data of Lee and Sanborn (ref. 15) and $\Delta H_0 = 198$ kcal/mol. This results in a computed C₃ number density of 8.89×10^{15} molecules/cm³ for the Brewer and Engelke experiment, whereas a number density of 2.15×10^{15} molecules/cm³ was obtained by

Brewer and Engelke using the free-energy functions of Pitzer and Clementi (ref. 20) and $\Delta H_0 = 188$ kcal/mol. Figure 12 shows that use of the revised number density brings the furnace data at 3200 K of reference 8 into good agreement with the present shock-tube data at $T = 3240$ K. It should be noted that the violet band system of CN and the Swan band system of C_2 were also observed by Brewer and Engelke but were "faired" out. (See fig. 1 of ref. 8.)

The data at 3240 K represent the lower temperature limit for the present experiment, since the equilibrium density program predicts that solid carbon will be present in the flow for lower temperatures. No effects of particulate carbon are observable in the data of figure 12. A discussion of tests designed to observe particulate carbon is contained in a subsequent section of the report.

No data were presented in reference 8 for wavelengths shorter than 370 nm. For less than 370 nm, the present data (figs. 11 and 12) show a continuation of the downward trend to about 300 nm, at which point the cross section becomes nearly constant (fig. 11). The data for this shortest wavelength region (below 300 nm) must be viewed with some skepticism. The light output of the xenon flash lamp was very low in this region, resulting in poor signal-to-noise ratio on the photomultiplier channels and susceptibility to stray light contamination. Also, insufficient data were obtained at these wavelengths to indicate whether the absorption was due to C_3 or some other species.

Temperature Variation of Absorption Cross Section

For each setting of the spectrograph grating, a number of runs were made with varying shock strengths, and thus, the temperature effect on absorption was determined at a number of wavelengths. A total of 26 different wavelengths was available with which to determine the temperature effect on absorption cross section. In figure 13, for six of these wavelengths the experimentally determined absorption cross section is shown over the temperature range of the experiment. Also shown for each wavelength is a least-squares curve fit to the data of the form

$$\sigma_\lambda = a_0 + a_1 T + a_2 T^2 + a_3 T^3 \quad (8)$$

The curve-fit equations may then be used to generate an approximate spectral absorption profile for any specified temperature within the temperature range of the experiment. Such profiles are presented for four selected temperatures in figure 14, where the value of equation (8) is shown at each wavelength by a symbol. The vertical bar shows the standard deviation of the data from the curve for that wavelength setting. Absence of a bar indicates insufficient data to determine standard deviation.

The spectral absorption curve fits shown in figure 14 indicate that for the temperature range 3400 to 4000 K, the profiles remain quite similar. However, there appears to be some change with temperature in the general amplitude. The amplitude is highest at the low temperature extreme (3400 K) and decreases to a minimum at about 3800 K. Figure 13 shows that this trend is displayed at most wavelengths, with the minimum usually occurring near 3800 K. At temperatures of

4000 K and above, the general trend is for the absorption cross section to rise, but the very limited data in this temperature range do not permit a firm conclusion.

It can be shown (e.g., ref. 21) that for a given atomic transition, the integral of the spectral absorption coefficient is proportional to the electronic oscillator strength. Thus,

$$\int_0^\infty K_\omega d\omega = \frac{\pi e^2}{mc^2} N f_e \quad (9)$$

in which ω is wave number, f_e is the electronic absorption oscillator strength, and N is the number density of the absorbing state. Now, as is done frequently, the concept of oscillator strength will be assumed to apply to an entire molecular transition, even though there are weaknesses in making this assumption. Since, for the present transition, the absorbing state is the ground state, N may be taken as the total number density of C_3 . Equation (9) may then be solved for f_e to give

$$f_e = 1.13 \times 10^{12} \int_0^\infty \sigma_\omega d\omega \quad (10)$$

For the present results, the integral of the absorption cross section was approximated by using the curve fits (eq. (8)) for each wavelength to define σ_ω as a function of temperature, and the integral was determined by using the trapezoid rule. For this calculation, certain wavelength channels were believed to be influenced by the C_2 Swan bands, and therefore, only 21 channels were included in the computation. The results of this computation are presented in figure 15. This figure shows that the oscillator strength varies over the temperature range of the experiments from about 0.062 at 3300 K to a minimum of 0.036 at about 3900 K. The average oscillator strength is 0.047 over the temperature range 3300 to 4200 K.

An estimate of the possible errors in the oscillator strength indicates that the greatest uncertainty lies in the calculation of C_3 number density in the flow. An uncertainty of ± 40 percent is assigned to this calculation, which is combined with an estimated maximum systematic error in the absorption measurement of ± 20 percent to yield an overall uncertainty of 60 percent.

Brewer and Engelke (ref. 8) calculate an oscillator strength f_e of 0.13 for their experiment. However, when their C_3 number density is recalculated according to the present recommendations (Lee and Sanborn's thermal properties (ref. 15) and $\Delta H_0 = 198$ kcal/mol), the oscillator strength becomes 0.031. The difference in this value and the value obtained in the present experiment is caused by the more extensive wave-number range over which the present absorption data are integrated.

Particulate Formation

One of the major concerns in the present experiments is whether solid particulates were present in the test stream. For the present test conditions, the ACE computer program predicts that solid carbon will be present if the postshock temperature is below about 3220 K. For this reason, the present tests used only runs for which the postshock temperature was computed to be 3300 K or greater, with the exception of the low-temperature survey presented in figure 12.

If thermochemical equilibrium was not achieved in the present tests, and as a result, the test stream contained particulate carbon, the absorption results would include the absorption and scattering of the particulates. Also, the actual concentration of carbon-bearing gaseous species would be lowered because of the loss of carbon to the solid state.

In order to examine the effects of particulate carbon in the test gas, a series of runs was made at postshock temperatures below 3220 K. Figure 16 shows examples of the absorption coefficients measured. As the temperature of the postshock test gas is decreased, the character of the spectral absorption profile changes: the absorption coefficient increases markedly for the short-wavelength portion of the spectrum. Thus, the absorption coefficient rises monotonically with decreasing wavelength at temperatures below 3000 K (fig. 16(c)); whereas at temperatures above 3200 K (e.g., fig. 16(a)), a maximum occurs near 400 nm, with decreasing absorption at shorter wavelengths.

The calculated effects of particulate absorption and scattering are also shown in figure 16. The absorption and scattering were calculated by the method described in reference 22. According to reference 22, most soot particles are either "spheres" or long strands with radii lying between 10 and 40 nm, and thus $2\pi a/\lambda \ll 1$, where a is the particle radius. For this "Rayleigh region" the absorption cross section $\sigma_{\lambda,abs}$ is given as

$$\sigma_{\lambda,abs} = p_{\lambda} \pi a^3$$

where p_{λ} is the so-called "Rayleigh factor." The absorption coefficient is then

$$K_{\lambda,abs} = N_p \sigma_{\lambda,abs} = \frac{3}{4} \frac{\bar{m}}{\rho_c} p_{\lambda}$$

where \bar{m} is the mass of particulates per unit flow volume and ρ_c is the density of carbon. Interpolated values for p_{λ} as a function of wavelength were obtained from the tabulated values given in reference 22.

The Rayleigh scattering cross section is given in reference 11 as

$$\sigma_{\lambda,sca} = \frac{24\pi^3 v^2}{\lambda^4} \frac{[(N_1^2 - N_2^2 - 1)(N_1^2 - N_2^2 + 2) + 4N_1^2 N_2^2]^2 + 36N_1^2 N_2^2}{[(N_1^2 - N_2^2 + 2)^2 + 4N_1^2 N_2^2]^2}$$

where V is the particle volume and $N_1 + iN_2$ is the complex refractive index of the carbon particles. Values for $N_1^2 - N_2^2$ and $2N_1N_2$ were obtained from reference 23. The contribution to the extinction coefficient due to Rayleigh scattering is then given by

$$K_{\lambda, \text{sca}} = N_p \sigma_{\lambda, \text{sca}} = \frac{3}{4} \frac{\bar{m}}{\rho_c \pi a^3} \sigma_{\lambda, \text{sca}}$$

In figure 16, the total contribution to the extinction coefficient due to particle absorption and scattering is shown for an assumed particle radius a of 30 nm. Since the absorption term dominates and is independent of particle radius, the resulting total is not very sensitive to assumed particle size. The calculated extinction coefficients have been reduced by a factor of 4 in order to compare them better with the experimental data. It is seen in figure 16 that the change in the nature of the experimental absorption profile as the temperature is reduced below 3000 K may be ascribed to the effects of particulate carbon. The fact that the extinction coefficient is lower by about a factor of 4 than the calculated level suggests that less particulate carbon is present in the experiment than is calculated. These results strongly suggest that no appreciable amount of particulate carbon is present at the higher temperatures for which the present experimental program was conducted.

CONCLUDING REMARKS

The spectral absorption properties of triatomic carbon C_3 have been measured in a shock tube containing a test-gas mixture of acetylene diluted with argon. The temperature behind the incident shock ranged from about 3240 to 4300 K, and the corresponding pressure varied from 37 to 229 kPa. Appreciable absorption was measured at wavelengths from about 300 nm to about 540 nm. Absorption was also noted below 300 nm, but the lack of sufficient data and the poor signal-to-noise ratio in this wavelength range precluded a firm determination that this short-wavelength absorption was due to C_3 .

The absorption profile was very similar to that measured by Brewer and Engelke (J. Chem. Phys., vol. 36, no. 4, Feb. 1962) in a furnace at 3200 K. They did not make measurements below 370 nm and thus did not include the short-wavelength portion of the profile determined in the present study. However, for the overlapping range of wavelengths of the two experiments, the results are in good agreement.

Data taken for a narrow passband at specific wavelengths over a range of temperature and pressure reveal a temperature variation of the spectral absorption cross section. Curve fits for these data were obtained for 21 wavelengths, and these curve fits can be used to construct approximate spectral profiles for any selected temperature within the valid range of the data. If such profiles are integrated with respect to wave number, an electronic oscillator strength is obtained for the transition. This oscillator strength varied from 0.062 to 0.036 over the temperature range 3300 to 4200 K and may be compared with a value of 0.13 quoted by Brewer and Engelke or a value of 0.031 if the number density of their experiment is reevaluated.

The absorption cross section is determined not only by the absorption coefficient measured, but also by the computed number density of the absorbing state. This latter quantity was computed in the present study by use of an equilibrium, free-energy-minimization computer program which assumed a value of the heat of formation for C₃ of 198 kcal/mol at a temperature of 0 K. The thermal properties of C₃ were taken from the calculations of Lee and Sanborn (High Temp. Sci., vol. 5, no. 6, Dec. 1973).

Solid carbon particulates were not expected to be present at the postshock temperatures of the present tests, on the basis of the equilibrium calculations. In order to examine the effects of particulates, a few runs were made at lower temperatures, where solid carbon was calculated to be a part of an equilibrium composition. As the temperature was decreased below 3000 K, the absorption profile underwent a distinct change and assumed a shape similar to that which is calculated for absorbing and scattering Rayleigh particles. The experimental profile was, however, lower than the calculated profile by about a factor of 4, suggesting that less carbon was in the solid state than was calculated. It was concluded, therefore, that in the present tests, the test gas at postshock temperature above 3300 K was free of solid carbon particulates.

Langley Research Center
National Aeronautics and Space Administration
Hampton, VA 23665
February 1, 1978

APPENDIX

THERMAL PROPERTIES OF C₃

The determination of the concentration of C₃ behind the shock wave for the present test conditions assumes that thermochemical equilibrium has been attained in the flow, and consists of minimizing the Gibbs free energy for the mixture of species which are present. This calculation requires a definition of the temperature-dependent thermodynamic properties for each species. In order to have a common reference point for all species, the enthalpy is referred to the elements in their most natural form at 298 K and a pressure of 1 atm. In this form, the equation for static enthalpy is

$$h \equiv \int_{298}^T c_p dT + \Delta H_{298}^\circ \quad (A1)$$

Equation (A1) shows that the heat of formation ΔH_{298}° is required for each species which is to be considered in the final mixture. In this appendix the available information on the thermodynamic properties and heat of formation of C₃ is reviewed in order to assess the uncertainty in calculated number densities. A thorough review of the state of knowledge of carbon vaporization as of 1969 is given in reference 24. This appendix attempts a much briefer review, but includes data and calculations published since 1969.

Evaluation of Vapor-Pressure Data

The heat of formation of C₃ has not been established to a satisfactory degree of accuracy, despite the number of experiments which have been conducted to determine this quantity. The experiments are based on the vaporization of graphite. The chief experimental difficulty is the determination of the fraction of total vapor pressure which is due to the partial pressure of C₃.

The vapor-pressure data are commonly analyzed by two methods, referred to as the second-law method and the third-law method. The second-law method makes use of the Clausius-Clapeyron equation, with assumptions that the vapor behaves as an ideal gas and the changes in specific volume of the solid are negligible (see, for example, ref. 25):

$$\Delta H_T^\circ = -R \frac{d(\ln p)}{d(1/T)} \quad (A2)$$

The logarithm of the experimental values of the partial pressure of C₃ is plotted against the inverse of the vapor temperature, and the heat of formation may thus be inferred from the slope of the line through the data.

The advantage of the second-law method lies in the fact that only relative values of pressure, not absolute values, are required. Since the partial pressure of C₃ is usually obtained from mass spectrometer readings, the scaling

APPENDIX

factors which are used to convert the spectrometer signal of the C₃ mass peak to partial pressure do not influence the slope of the curve. The chief disadvantage of this method is that the equation yields the heat of formation at the temperature T of the pressure measurements. Now if only a small range of temperature is used in the experiments, an accurate determination of the slope of the line through the data is difficult. If a wide range of temperature is used in the experiment, the data may not be expected to be along a straight line, since the heat of formation is, in general, temperature dependent.

The heat of formation at the temperature T may be converted to the value at the reference temperature by Kirchhoff's equation:

$$\Delta H_{\text{ref}}^{\circ} = \Delta H_T^{\circ} + (h_T - h_{\text{ref}})_{\text{solid}} - (h_T - h_{\text{ref}})_{\text{vapor}} \quad (\text{A3})$$

where the subscripts ref and T denote the reference temperature and the given temperature. Both 0 K and 298.15 K have been used as the reference temperature. However, data based on one reference temperature may be converted to another reference by equation (A3). Note that equation (A3) requires a knowledge of the enthalpy-temperature variation for both the vapor and solid states.

The third-law method makes use of the free-energy function and may be written

$$\frac{\Delta H_{\text{ref}}^{\circ}}{T} = -R \ln p + \left(\frac{G_T - h_{\text{ref}}}{T} \right)_{\text{solid}} - \left(\frac{G_T - h_{\text{ref}}}{T} \right)_{\text{vapor}} \quad (\text{A4})$$

Reference 26 discusses the evaluation of vaporization data by the second-law and third-law methods. Although the third law allows a determination of the heat of formation from a single measurement, it requires a knowledge of the Gibbs free energy for both the vapor and solid states. Furthermore, the calculation now depends upon an absolute determination of the species vapor pressure p.

It is common practice to evaluate a set of data by both the second-law and the third-law methods, to note the consistency of results. However, the results of the third-law method are to be preferred over those of the second-law method, because evaluation of each data point is independent of the others. This allows trends with temperature or inconsistent data points to be noted more easily.

The foregoing discussion has reviewed these data evaluation methods in order to emphasize the importance of an accurate knowledge of the thermodynamic properties of the species under study. Specifically, the enthalpy and Gibbs free energy must be known over the temperature range of interest, and if a change is made in the assumed variation of enthalpy and Gibbs energy with temperature, the data will yield a different value of heat of formation.

Thermodynamic Functions of C₃

The free-energy function for C₃ was calculated by Glockler (ref. 27) in 1954. He assumed a multiplicity of 5 for the ground state and a bending fre-

APPENDIX

quency of 353 cm^{-1} and estimated the heat of formation as 212.3 kcal/mol. His calculation was based on the standard rigid-rotor harmonic-oscillator model. In 1959 Pitzer and Clementi (ref. 20) corrected the multiplicity of the ground state to 1 and recomputed the free-energy function and the enthalpy using a bending frequency of 550 cm^{-1} . However, in 1965 Gausset, Herzberg, Lagerqvist, and Rosen (ref. 3) published a detailed spectroscopic analysis of C_3 , concluding that the bending frequency of the ground electronic state was of the order of 65 cm^{-1} for the first few levels. This low bending frequency created a difficulty in calculating the thermal functions, for as shown by Robiette and Strauss (ref. 28), the assumption of a harmonic oscillator with the lower value of bending frequency causes the calculated entropy to be too high compared with that obtained from the temperature measurements. For example, Thorn and Winslow (ref. 29) calculated a value of entropy S_{2400} of 77.41 eu from their vapor-pressure measurement, and Robiette and Strauss (ref. 28) interpreted the pressure measurements of Drowart et al. (ref. 13) to yield $S_{2400} = 76.1$ eu. Robiette and Strauss showed, however, that at 2400 K a harmonic-oscillator calculation with a bending frequency of 63 cm^{-1} yields an entropy of 85.56 eu. They showed that the entropy can be reduced by about 3 eu by taking the quartic anharmonicity into account.

Strauss and Thiele (ref. 30) calculated the thermal properties of C_3 using the spectroscopic data of Gausset et al. (ref. 3) and accounting for rotation-vibration interaction. However, as they pointed out, only the first few levels of the bending vibration have been measured, so that the potential function must be based on a very limited set of energy levels. They show that inclusion of the quartic anharmonicity lowers the entropy at 2400 K by about 2.8 eu, and inclusion of the vibration-rotation coupling lowers it by another 1.1 eu, to a value of 81.4. Further, they demonstrated that even if the potential increased drastically above a bending angle of 0.4π , the calculated entropy cannot be lowered below $S_{2400} = 79.8$ eu. It appears therefore, that the best calculation method cannot compute entropy values as low as those inferred from the experiments of references 13 and 29.

The JANAF tables (ref. 26) adopted a potential function which makes use of the vibrational frequencies measured by Gausset et al. (ref. 3) for the low levels and then steepens to fit a vibrational frequency interval of 650 cm^{-1} for higher levels. The value of 650 cm^{-1} is admitted to be arbitrary and was selected to yield functions which approximate experimental data. Their value of entropy at 2400 K is $S_{2400} = 78.4$ eu.

Hansen and Pearson (ref. 31) used a quadratically perturbed square well potential in a quantum calculation to approximate the spectroscopic data of C_3 . The maximum molecular bending at the potential wall was 64° for this model, which is in close agreement with Strauss and Thiele's approximate model (ref. 30), which steepened the potential at a bending angle of 0.4π rad, or 72° . From their analysis, Hansen and Pearson calculated an entropy at 2400 K of $S_{2400} = 79.68$ eu, and concluded that their limiting calculation thereby supports the calculation of Strauss and Thiele.

Lee and Sanborn (ref. 15) also calculated the thermal properties of C_3 by developing a special potential model. Their anharmonic model for the lower

APPENDIX

vibrational levels fits the data of Gausset et al. (ref. 3), and for higher vibrational levels the term difference approaches 308 cm^{-1} , the bending frequency of the first excited state. They also included the electronic contribution to the partition function, which had been neglected in the other treatments. However, they used a rigid-rotor assumption and thus neglected vibration-rotation interaction. Lee and Sanborn showed that their results are in close agreement with those of Strauss and Thiele (ref. 30) when they omitted the electronic contribution. They used the electronic energy levels given by Pitzer and Clementi (ref. 20) in computing the electronic contribution to the partition function.

Figure 17 compares the specific heat at constant pressure, the enthalpy, the entropy, and the Gibbs energy function as calculated by references 15, 26, 30, and 31. The differences between the calculations are most accentuated in c_p , but are appreciable in the other functions as well. The Gibbs functions as computed by Lee and Sanborn are seen to be quite close to those by Strauss and Thiele throughout the temperature range. About half the difference between these curves may be attributed to the electronic contribution which Lee and Sanborn included.

The calculations of Strauss and Thiele (ref. 30) would appear to be the most rigorous treatment of the C_3 molecule with the spectroscopic data available, except for omission of the electronic contribution to the partition function. Since the results of Lee and Sanborn are in acceptable agreement with the results of Strauss and Thiele when the electronic contribution is omitted, their thermal functions (ref. 15) seem to be the best choice. Lee and Sanborn also presented thermal functions for C_4 through C_7 . In addition, the properties for C_1 and C_2 were extended to 10 000 K. Thus a consistent set of properties for the carbon species up to C_7 are available in reference 15 for carbon vapor calculations.

For the reasons stated, the equilibrium calculations of this study used curve fits to the calculated data of Lee and Sanborn for the thermodynamic functions of C_3 .

One further point of interest may be noted regarding the evaluation of the various calculations of thermal properties. The most nagging problem has been the fact that each of the calculations yielded higher entropy values than those measured by Drowart et al. (ref. 13) and Thorn and Winslow (ref. 29), and resolving the low bending frequency with the experimental entropy values seemed impossible. In 1972, however, Wachi and Gilmartin (ref. 32) made new vapor-pressure measurements with a calibrated mass spectrometer and a Knudsen effusion cell. They quoted experimental entropies at 2400 and 2700 K as $S_{2400} = 81.47 \text{ eu}$ and $S_{2700} = 82.91 \text{ eu}$. These values are shown in figure 17(c) and are in excellent agreement with the calculation of Strauss and Thiele (ref. 30) and in acceptable agreement with the calculation of Lee and Sanborn (ref. 15). Thus, if one assumes that the measurements of Wachi and Gilmartin are superior to the earlier ones, the discrepancy between theory and experiment is resolved on this point.

APPENDIX

Heat of Formation of C₃

In the previous section, reasons were given for choosing the calculated data of Lee and Sanborn (ref. 15) for curve fitting the equilibrium calculations of the present study. Having made a choice, the various experimental vapor-pressure measurements may now be compared using the same thermal property data for each. In addition to the measurements of Drowart et al. (ref. 13), mass spectrometer measurements have also been made by Wachi and Gilmartin (ref. 32), by Milne et al. (ref. 33), and by Zavitsanos and Carlson (ref. 34).

The conversion of mass spectrometer signal level to partial pressure requires several conversion factors relating to ionization cross section, secondary electron yields of the electron multiplier, and spectrometer transmission coefficient. In reference 35, Meyer and Lynch made a careful evaluation of the factors affecting spectrometer response, recommended new conversion factors, and reevaluated the data of references 13 and 34. They also included the data of reference 32, but since Wachi and Gilmartin used gold and cobalt to calibrate their mass spectrometer, their conversion factors were not revised. Meyer and Lynch then used the thermal properties of Strauss and Thiele (ref. 30) to reduce the data.

In the present study the conversion factors of Meyer and Lynch (ref. 35) were adopted and applied to the data of references 13, 33, and 34. The data of Wachi and Gilmartin (ref. 32) were used without correction. The resulting partial pressure of C₃ is shown in figure 18 as a function of the inverse temperature 1/T.

It was deemed highly desirable to include data obtained by a different method, and in a different temperature range; therefore, the data of Lundell and Dickey (ref. 36) have also been included in figure 18. Lundell and Dickey used a powerful laser to vaporize graphite, and inferred the total vapor pressure from the surface recession rate. Figure 18 includes the five data points for which Lundell and Dickey state that the condition of pure carbon vapor at the surface was achieved. The partial pressure of C₃ was computed by subtracting the calculated partial pressures of C and C₂ from the total vapor pressure. The contributions of C₄ and larger molecules are expected to be negligible; however, note that neglect of these species means that the pressure shown in figure 18 for these data is an upper limit for the partial pressure of C₃.

All the vapor-pressure data shown in figure 18 were reduced to heat of formation by using the third-law method (eq. (A4)) and the thermal properties of Lee and Sanborn (ref. 15). For the thermal properties of solid state carbon, the curve fits of Gordon and McBride (ref. 37), which fit the values given in the JANAF tables (ref. 26), were used.

The average value of heat of formation for all data shown in figure 18 is $\Delta H_0^\circ = 197.85$ kcal/mol. However, it may be argued that this method of averaging tends to bias toward the experiments with the most data points; therefore, the data were also averaged by experimenter. The results are shown in the table on the following page and give an average of $\Delta H_0^\circ = 199.50$ kcal/mol. Determination of a second-law value does not appear to be helpful. Since the heat of formation varies with temperature, and since the composite data cover a wide

APPENDIX

Investigators	Average ΔH_0° , kcal/mol
Drowart, Burns, DeMaria, and Inghram (ref. 13)	197.25
Wachi and Gilmartin (ref. 32)	200.84
Zavitsanos and Carlson (ref. 34)	198.73
Milne, Beachey, and Greene (ref. 33)	196.22
Lundell and Dickey (ref. 36)	204.48
Average	199.50
Overall average of all data points	197.85

temperature range, a single straight-line fit is not meaningful. Moreover, the local slope of a curve fit through the data is very dependent on the analytical form of the assumed curve. In order to illustrate the curvature of a constant ΔH_0 curve, three computed curves are shown in figure 18 for constant values of $\Delta H_0 = 194$, 198, and 202 kcal/mol.

The conclusion drawn from this reexamination of carbon data is that the range of values for the heat of formation of C_3 which may be defended is from 197.85 to 199.50 kcal/mol. A value of 198 kcal/mol was selected for the present study and incorporated into the computer code which was used to determine C_3 number densities for the test conditions.

REFERENCES

1. Moss, James N.; Anderson, E. Clay; and Bolz, Charles W., Jr.: Viscous-Shock-Layer Solution With Radiation and Ablation Injection for Jovian Entry. AIAA Paper No. 75-671, May 1975.
2. Marr, G. V.; and Nicholls, R. W.: The Emission of the ' $\lambda 4050\text{\AA}$ ' Bands and an Associated Violet Continuum in Oxyacetylene Flames. Canadian J. Phys., vol. 33, no. 7, July 1955, pp. 394-396.
3. Gausset, L.; Herzberg, G.; Lagerqvist, A.; and Rosen B.: Analysis of the 4050-A Group of the C_3 Molecule. Astrophys. J., vol. 142, no. 1, July 1, 1965, pp. 45-76.
4. Weltner, W., Jr.; Walsh, P. N.; and Angell, C. L.: Spectroscopy of Carbon Vapor Condensed in Rare-Gas Matrices at 40° and 20° K. I. J. Chem. Phys., vol. 40, no. 5, Mar. 1964, pp. 1299-1305.
5. Weltner, William, Jr.; and McLeod, Donald, Jr.: Spectroscopy of Carbon Vapor Condensed in Rare-Gas Matrices at 40° and 20° K. II. J. Chem. Phys., vol. 40, no. 5, Mar. 1964, pp. 1305-1316.
6. Weltner, William, Jr.; and McLeod, Donald, Jr.: Spectroscopy of Carbon Vapor Condensed in Rare-Gas Matrices at 40° K. III. J. Chem. Phys., vol. 45, no. 8, Oct. 1966, pp. 3096-3105.
7. Barger, R. L.; and Broida, H. P.: Spectra of C_3 in Solidified Gases at 40° and 20° K. J. Chem. Phys., vol. 43, no. 7, Oct. 1965, pp. 2364-2370.
8. Brewer, Leo; and Engelke, John L.: Spectrum of C_3 . J. Chem. Phys., vol. 36, no. 4, Feb. 15, 1962, pp. 992-998.
9. Jones, Jim J.; Boughner, Robert E.; Haggard, Kenneth V.; Nealy, John E.; Schryer, David R.; and Zoby, Ernest V.: Radiative Property Data for Venusian Entry - A Compendium. NASA SP-348, 1974.
10. Nealy, John E.: Performance and Operating Characteristics of the Arc-Driven Langley 6-Inch Shock Tube. NASA TN D-6922, 1972.
11. Siegel, Robert; and Howell, John R.: Thermal Radiation Heat Transfer. Volume III - Radiation Transfer With Absorbing, Emitting, and Scattering Media. NASA SP-164, 1971.
12. Powars, Charles A.; and Kendall, Robert M.: User's Manual - Aerotherm Chemical Equilibrium (ACE) Computer Program. Aerotherm Corp., May 1969.
13. Drowart, J.; Burns, R. P.; DeMaria, G.; and Inghram, Mark G.: Mass Spectrometric Study of Carbon Vapor. J. Chem. Phys., vol. 31, no. 4, Oct. 1959, pp. 1131-1132.

14. Zavitsanos, P. D.: The Vaporization of Pyrolytic Graphite. Tech. Inform. Ser. No. R66SD31 (Contract AF 04(694)-222), Missile & Space Div., General Electric Co., May 1966. (Available from DDC as AD 633 611.)
15. Lee, E. L.; and Sanborn, R. H.: Extended and Improved Thermal Functions for the Gaseous Carbon Species C₁-C₇ From 298 to 10,000° K. High Temp. Sci., vol. 5, no. 6, Dec. 1973, pp. 438-453.
16. Woodward, Henry T.: Predictions of Shock-Layer Radiation From Molecular Band Systems in Proposed Planetary Atmospheres. NASA TN D-3850, 1967.
17. Mirels, H.: Flow Nonuniformity in Shock Tubes Operating at Maximum Test Times. Phys. Fluids, vol. 9, no. 10, Oct. 1966, pp. 1907-1912.
18. Mirels, Harold: Shock Tube Test Time Limitation Due to Turbulent-Wall Boundary Layer. AIAA J., vol 2, no. 1, Jan. 1964, pp. 84-93.
19. Main, Roger P.; and Bauer, Ernest: Equilibrium Opacities of Selected Materials at High Temperatures. Publ. No. U-3304 (Contract AF 29 (601)-7032), Aeronutronic, Oct. 1965.
20. Pitzer, Kenneth S.; and Clementi, Enrico: Large Molecules in Carbon Vapor. J. American Chem. Soc., vol. 81, no. 17, Sept. 1959, pp. 4477-4485.
21. Bates, D. R., ed.: Atomic and Molecular Processes. Academic Press, 1962.
22. Main, Roger P.; and Bauer, Ernest: Opacities of Carbon-Air Mixtures at Temperatures From 3000-10,000° K. J. Quant. Spectros. & Radiat. Transfer, vol. 6, no. 1, Jan./Feb. 1966, pp. 1-30.
23. Stull, V. Robert; and Plass, Gilbert N.: Emissivity of Dispersed Carbon Particles. J. Opt. Soc. America, vol. 50, no. 2, Feb. 1960, pp. 121-129.
24. Palmer, Howard B.; and Shelef, Mordecai: Vaporization of Carbon. Chemistry and Physics of Carbon, Volume 4, Philip L. Walker, Jr., ed., Marcel Dekker, Inc., 1968, pp. 85-135.
25. Zemansky, Mark W.: Heat and Thermodynamics. McGraw-Hill Book Co., Inc., 1943.
26. JANAF Thermochemical Tables. NSRDS-NBS 37, U.S. Dep. Commer., June 1971.
27. Glockler, George: The Heat of Sublimation of Graphite and the Composition of Carbon Vapor. J. Chem. Phys., vol. 22, no. 2, Feb. 1954, pp. 159-161.
28. Robiette, A. G.; and Strauss, H. L.: Third-Law Entropy of C₃. J. Chem. Phys., vol. 44, no. 7, Apr. 1, 1966, pp. 2826-2827.
29. Thorn, R. J.; and Winslow, G. H.: Vaporization Coefficient of Graphite and Composition of the Equilibrium Vapor. J. Chem. Phys., vol. 26, no. 1, Jan. 1957, pp. 186-196.

30. Strauss, Herbert L.; and Thiele, Everett: Thermodynamics of C₃. II. General Methods for Nonrigid Molecules at High Temperature. J. Chem. Phys., vol. 46, no. 7, Apr. 1967, pp. 2473-2480.
31. Hansen, C. Frederick; and Pearson, Walter E.: A Quantum Model for Bending Vibrations and Thermodynamic Properties of C₃. Canadian J. Phys., vol. 51, no. 1, Apr. 1, 1973, pp. 751-760.
32. Wachi, F. M.; and Gilmartin, D. E.: Heat of Formation and Entropy of C₃ Molecule. High Temp. Sci., vol. 4, no. 6, Dec. 1972, pp. 423-431.
33. Milne, Thomas A.; Beachey, Jacob E.; and Greene, Frank T.: Vaporization Kinetics and Thermodynamics of Graphite Using the High Pressure Mass Spectrometer. AFML-TR-74-57, U.S. Air Force, May 1974. (Available from DDC as AD 785 136.)
34. Zavitsanos, P. D.; and Carlson, G. A.: Experimental Study of the Sublimation of Graphite at High Temperatures. J. Chem. Phys., vol. 59, no. 6, Sept. 15, 1973, pp. 2966-2973.
35. Meyer, R. T.; and Lynch, A. W.: Reevaluation of Carbon Vapor Pressures and Third Law Heats of Formation: Triatomic Carbon. High Temp. Sci., vol. 5, no. 3, June 1973, pp. 192-204.
36. Lundell, John H.; and Dickey, Robert R.: Vaporization of Graphite in the Temperature Range of 4000° to 4500° K. AIAA 76-166 No. 76-166, Jan. 1976.
37. Gordon, Sanford; and McBride, Bonnie J.: Computer Program for Calculation of Complex Chemical Equilibrium Compositions, Rocket Performance, Incident and Reflected Shocks, and Chapman-Jouguet Detonations. NASA SP-273, 1971.

TABLE I.- SHOCK-TUBE INSTRUMENTATION PORT LOCATIONS AND TYPE OF DETECTOR

Station	Distance from diaphragm, m	Detector (a)
1	2.889	H.T.
2	4.417	P.
3	5.925	P.
4	7.447	H.T.
5	8.357	P.M.
6	8.662	P.
7	9.566	P.
8	11.092	P.
9	12.617	H.T.
10	14.126	P.
11 (test window)	14.940	P.M.
12	15.149	P.

^aAbbreviation for type of detector:

H.T. thin-film heat-transfer gage

P. pressure transducer

P.M. photomultiplier

TABLE II.- TEST CONDITIONS AND MEASURED ABSORPTION CROSS SECTIONS

FOR TEST-GAS MIXTURE: 2.99 PERCENT C₂H₂, 97.01 PERCENT ARGON

Run	V _s , m/sec	T ₅₀ , K	P ₅₀ , kPa	(N _{C₃}) ₅₀ × 10 ⁻¹⁶	λ, nm, and σ _λ × 10 ¹⁸ , cm ² ,* for spectrograph channel -							
					1	2	3	4	5	6	7	8
1	2237	3709	105	2.22	254	266	282	297	311	325	340	353
					1.30	1.45	1.80	1.61	1.87	2.16	2.70	2.80
2	2240	3717	105	2.23	289	302	317	333	346	360	375	388
					1.80	1.50	2.20	2.50	3.00	3.60	4.40	3.90
3	2237	3709	104	2.21	325	337	352	268	381	395	410	423
					2.23	2.34	2.86	3.32	3.90	3.37	2.38	1.64
4	2256	3771	106	2.24	360	373	388	403	416	430	445	458
					2.77	3.28	3.18	2.80	1.65	1.15	0.87	0.96
5	2221	3676	103	2.17	396	408	423	438	451	465	480	493
					4.17	2.72	1.61	1.13	0.82	1.78	0.26	0.51
6	2226	3688	103	2.19	431	444	459	473	486	500	515	528
					1.55	0.81	0.98	0.47	0.30	0.70	2.56	0.41
7	2224	3682	103	2.14	466	479	494	508	521	535	550	563
					1.93	0.23	0.20	1.46	0.17	0.12	0.49	0
8	2157	3550	110	2.07	-----	-----	397	426	454	482	512	537
					-----	-----	4.87	2.04	0.72	0.58	1.83	0.47
9	2149	3532	109	2.02	-----	-----	397	426	454	482	512	537
					-----	-----	5.39	2.46	1.01	1.17	2.14	1.03
10	2152	3540	109	2.04	-----	-----	397	426	454	482	512	537
					-----	-----	5.83	2.67	1.22	1.05	2.14	0.94

*For each spectrograph channel and each run, λ is given on the top line;
σ, on the bottom line.

TABLE II.- Continued

Run	V _S , m/sec	T ₅₀ , K	P ₅₀ , kPa	(N _{C₃}) ₅₀ × 10 ⁻¹⁶	λ , nm, and $\sigma_{\lambda} \times 10^{18}$, cm ² ,*							
					1	2	3	4	5	6	7	8
11	2046	3375	196	2.15	-----	-----	397	426	454	482	512	537
					-----	-----	5.90	2.66	1.59	1.06	1.36	0.55
12	2224	3722	163	3.23	-----	-----	397	426	454	482	512	537
					-----	-----	3.81	1.97	0.92	0.69	1.35	0.67
13	2210	3724	229	4.23	-----	-----	397	426	454	482	512	537
					-----	-----	4.43	1.91	0.87	0.53	1.13	0.47
14	2509	4229	78	0.82	-----	-----	397	426	454	482	512	537
					-----	-----	4.38	3.44	1.27	1.22	5.30	3.16
15	2136	3565	214	3.32	-----	-----	397	426	454	482	512	537
					-----	-----	4.97	2.62	1.16	1.22	1.65	0.65
16	2217	3676	117	2.39	-----	-----	405	434	461	490	520	545
					-----	-----	3.92	1.55	0.69	0.50	0.49	0.11
17	2209	3662	116	2.36	-----	-----	405	434	461	490	520	545
					-----	-----	4.13	1.64	0.98	0.64	0.98	0.67
18	2246	3708	84	1.83	-----	-----	405	434	461	490	520	545
					-----	-----	3.08	1.41	1.20	0.28	1.03	-----
19	2454	4088	58	0.79	-----	-----	405	434	461	490	520	545
					-----	-----	2.16	1.12	2.06	0.50	1.68	1.68
20	2170	3638	222	3.78	-----	-----	405	434	461	490	520	545
					-----	-----	3.59	1.76	0.84	0.73	1.16	0.64

*For each spectrograph channel and each run, λ is given on the top line;
 σ , on the bottom line.

TABLE II.- Continued

Run	V_s , m/sec	T_{50} , K	P_{50} , kPa	$(N_{C_3})_{50} \times 10^{-16}$	λ , nm, and $\sigma_\lambda \times 10^{18}$, cm ² , * for spectrograph channel -							
					1	2	3	4	5	6	7	8
21	2317	3896	128	2.60	----	----	405	434	461	490	520	545
					----	----	3.68	1.55	0.98	0.67	1.57	1.13
22	2429	4103	102	1.58	----	----	405	434	461	490	520	545
					----	----	3.64	2.05	2.24	----	2.69	2.04
23	2288	3721	37	0.86	----	----	405	434	461	490	520	545
					----	----	2.95	1.19	0.82	0.65	0.26	0.49
24	2117	3411	53	1.06	----	----	405	434	461	490	520	545
					----	----	4.97	1.82	----	0.61	0.27	0.57
25	2096	3380	62	1.12	----	----	405	434	461	490	520	545
					----	----	4.49	1.71	0.49	0.40	0.29	0.43
26	2573	4328	65	0.43	----	----	405	434	461	490	520	545
					----	----	7.43	6.23	5.45	2.71	4.21	5.99
27	2506	4224	79	0.85	----	----	405	434	461	490	520	545
					----	----	3.29	2.96	1.47	1.06	3.50	
28	2434	4112	99	1.52	----	----	405	434	461	490	520	545
					----	----	4.83	2.47	2.06	0.91	1.65	2.23
29	2237	3721	119	2.48	----	----	405	434	461	490	520	545
					----	----	4.66	1.70	0.98	0.76	0.46	1.10
30	2243	3759	178	3.56	----	----	405	434	461	490	520	545
					----	----	4.09	1.66	0.85	0.37	0.45	0.78

*For each spectrograph channel and each run, λ is given on the top line;
 σ , on the bottom line.

TABLE II.- Continued

Run	V _s , m/sec	T ₅₀ , K	P ₅₀ , kPa	(N _{C3}) ₅₀ × 10 ⁻¹⁶	λ, nm, and σ _λ × 10 ¹⁸ , cm ² , * for spectrograph channel -							
					1	2	3	4	5	6	7	8
31	2137	3543	161	2.67	----	----	405	434	461	490	520	545
					----	----	6.31	2.11	1.23	0.63	0.54	0.85
32	2074	3433	201	2.50	----	----	405	434	461	490	520	545
					----	----	6.03	2.18	1.10	0.59	0.68	0.76
33	2340	3946	130	2.56	301	314	329	344	357	371	386	400
					1.48	1.70	2.54	2.33	2.97	2.33	3.92	2.65
34	2430	4105	102	1.58	301	314	329	344	357	371	386	400
					1.30	2.12	1.78	2.51	3.95	4.10	5.26	2.71
35	2463	4109	59	0.76	301	314	329	344	357	371	386	400
					1.48	2.09	2.46	2.22	5.05	4.43	7.56	3.85
36	2220	3686	118	2.42	301	314	329	344	357	371	386	400
					1.60	1.80	2.35	2.36	2.60	3.12	4.28	3.31
37	2082	3429	153	2.11	301	314	329	344	357	371	386	400
					2.35	2.67	3.35	3.84	4.33	4.69	5.60	5.42
38	2102	3379	53	1.00	301	314	329	344	357	371	386	400
					2.16	2.26	2.69	3.56	4.25	4.60	5.36	3.67
39	2202	3492	47	1.08	301	314	329	344	357	371	386	400
					1.31	1.72	2.22	2.32	3.53	3.13	4.34	2.99
40	2104	3398	63	1.16	301	314	329	344	357	371	386	400
					1.49	2.06	2.88	3.32	3.76	3.81	5.86	3.94

*For each spectrograph channel and each run, λ is given on the top line; σ, on the bottom line.

TABLE II.- Concluded

Run	V_s , m/sec	T_{50} , K	P_{50} , kPa	$(N_{C_3})_{50} \times 10^{-16}$	λ , nm, and $\sigma_\lambda \times 10^{18}$, cm ² ,* for spectrograph channel -							
					1	2	3	4	5	6	7	8
41	2221	3666	116	2.37	-----	-----	256	272	285	299	314	328
					-----	-----	2.60	2.00	0.90	1.40	1.50	1.78
42	2309	3845	89	1.86	-----	-----	256	272	285	299	314	328
					-----	-----	1.70	1.58	1.24	0.80	1.54	1.56
43	2082	3370	59	1.01	-----	-----	256	272	285	299	314	328
					-----	-----	3.20	2.50	1.60	1.51	2.46	2.30
44	2038	3264	59	0.864	287	299	314	329	343	357	371	385
					-----	-----	-----	3.69	4.26	5.39	6.37	6.46
45	2035	3260	58	0.854	325	338	352	368	381	395	409	423
					2.67	4.10	5.10	6.03	6.04	6.62	4.33	2.35
46	2026	3242	58	0.807	360	373	388	403	416	430	445	458
					6.12	6.30	6.97	6.21	-----	2.35	1.03	0.58
47	2026	3242	59	0.823	431	444	458	474	487	501	515	529
					2.06	0.75	0.76	1.60	0.30	0.40	2.10	0.13
48	2011	3212	57	0.748	395	408	423	438	452	465	480	494
					6.88	4.45	2.39	1.73	0.70	1.58	0.57	0.56
49	2017	3221	57	0.769	466	479	494	509	522	536	551	564
					1.87	0.79	0.52	1.71	0.64	0.63	0.67	1.40

*For each spectrograph channel and each run, λ is given on the top line;
 σ , on the bottom line.

TABLE III.- TEST CONDITIONS AND MEASURED ABSORPTION CROSS SECTIONS

FOR TEST-GAS MIXTURE: 1.97 PERCENT C₂H₂, 98.03 PERCENT ARGON

Run	V _s , m/sec	T ₅₀ , K	p ₅₀ , kPa	(N _{C3}) ₅₀ × 10 ⁻¹⁶	λ, nm, and σ _λ × 10 ¹⁸ , cm ² , * for spectrograph channel -							
					1	2	3	4	5	6	7	8
50	2348	4147	78	0.52	----	----	405	434	461	490	520	545
					----	----	2.00	0.93	1.75	0.30	----	2.30
51	2315	4084	89	0.76	----	----	405	434	461	490	520	545
					----	----	2.00	0.73	1.20	----	----	1.39
52	2295	3670	87	1.06	----	----	405	434	461	490	520	545
					----	----	2.14	1.16	0.82	0.30	0.20	0.77
53	2193	3820	112	1.60	----	----	405	434	461	490	520	545
					----	----	3.60	1.80	1.00	----	0.40	1.10
54	2211	3863	114	1.57	----	----	405	434	461	490	520	545
					----	----	2.40	0.90	0.50	0.24	0.10	0.94
55	2082	3580	151	2.02	----	----	405	434	461	490	520	545
					----	----	3.78	1.49	0.77	0.27	0.32	0.70
56	2127	3687	158	2.27	----	----	405	434	461	490	520	545
					----	----	3.30	1.26	0.96	0.14	0.31	0.49
57	2052	3525	195	2.25	----	----	405	434	461	490	520	545
					----	----	4.88	1.61	0.60	0.25	0.38	0.63
58	2049	3511	171	1.03	----	----	405	434	461	490	520	545
					----	----	5.00	1.88	0.88	0.71	0.47	0.55
59	2157	3753	137	2.01	----	----	405	434	461	490	520	545
					----	----	2.81	1.28	0.77	0.34	0	0.56

*For each spectrograph channel and each run, λ is given on the top line;
σ, on the bottom line.

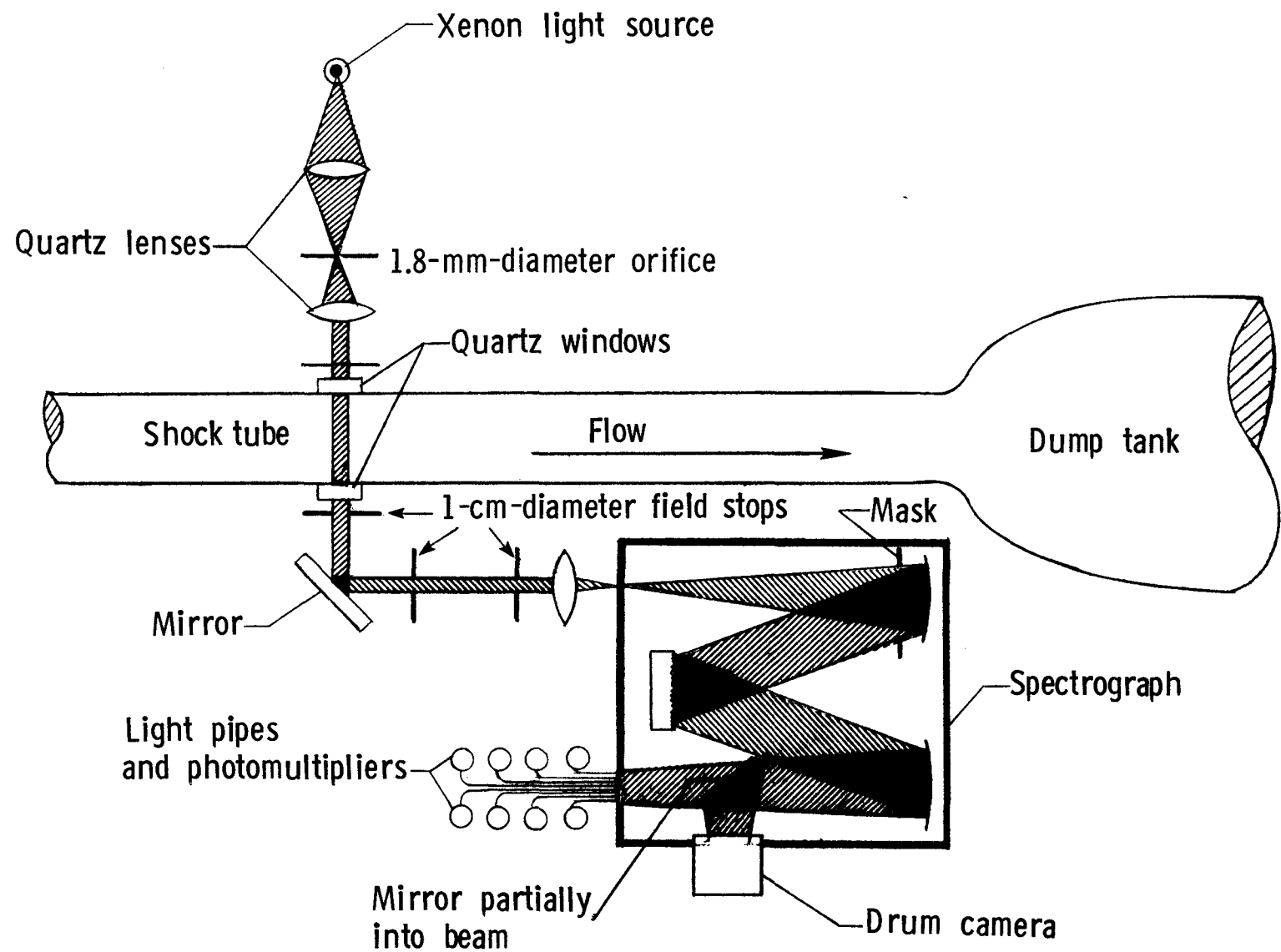


Figure 1.- Schematic of shock-tube test location and optical arrangement.

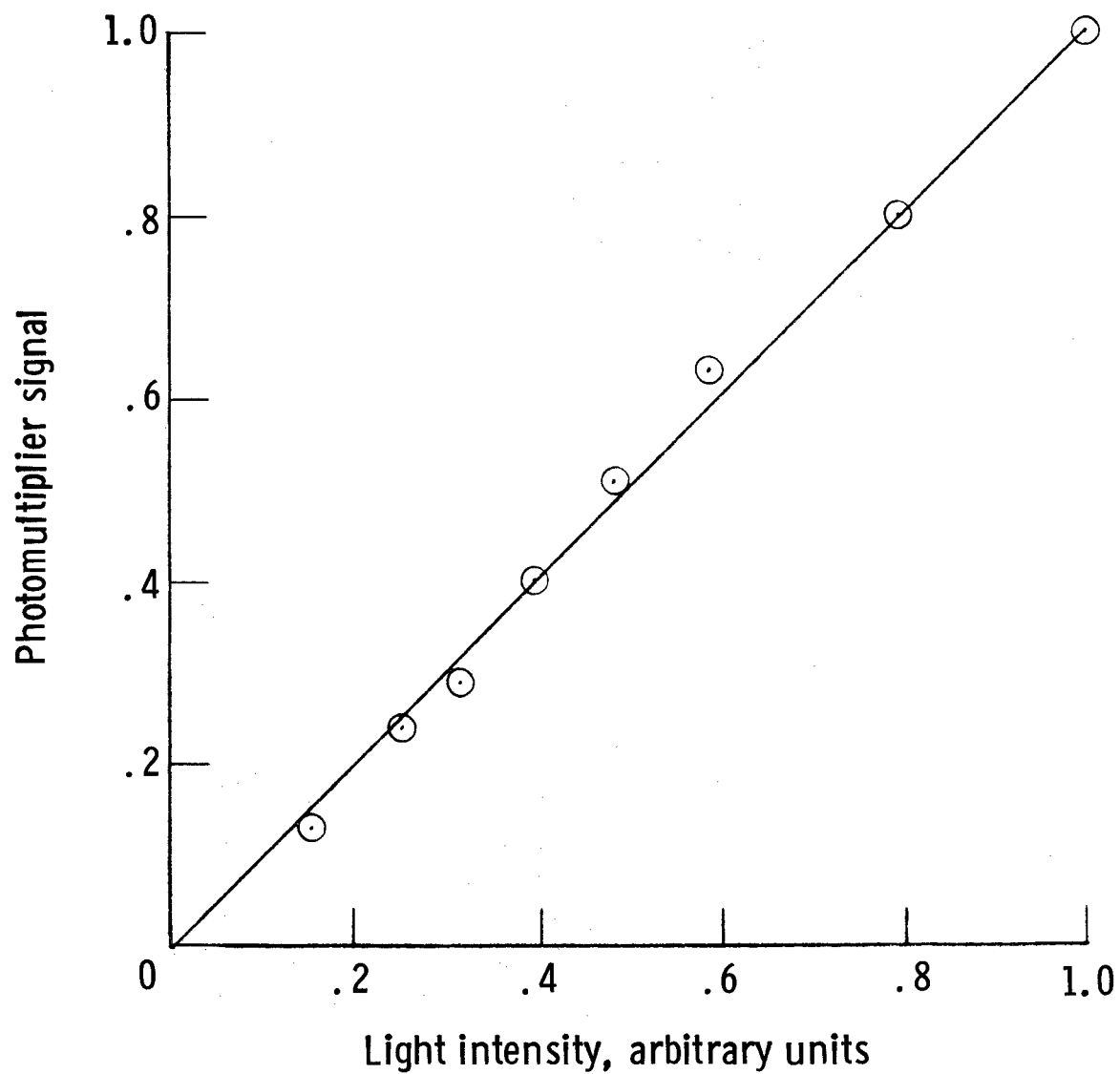
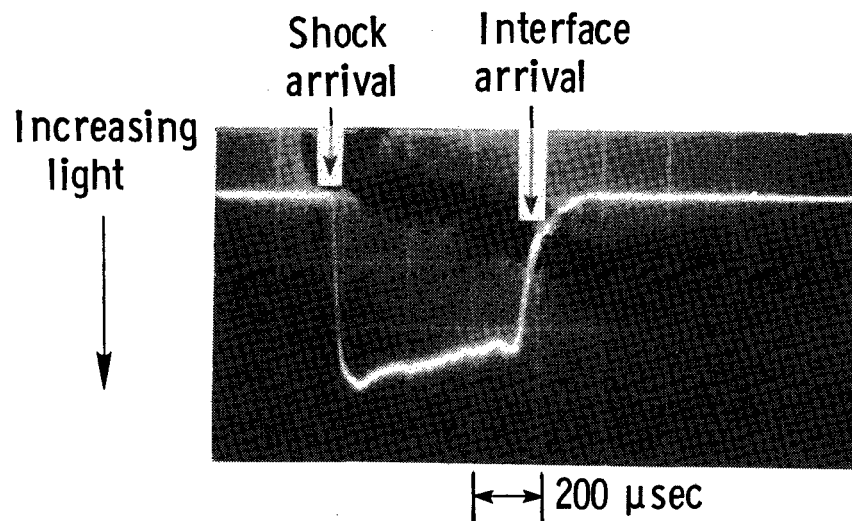
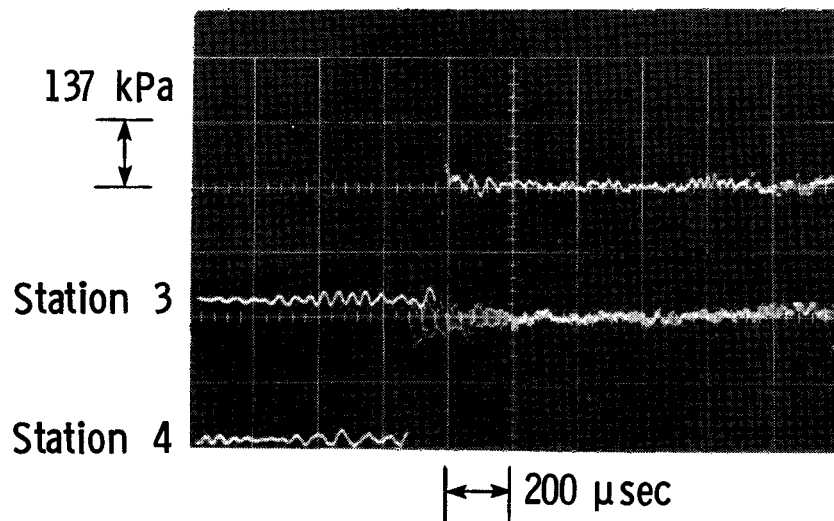


Figure 2.- Example of photomultiplier linearity check.



(a) Photomultiplier traces.



(b) Sample pressure transducer traces. (Note that the traces have different start times.)

L-78-15

Figure 3.- Sample oscillograms showing photomultiplier and pressure transducers as shock detectors. $p_2 = 221 \text{ kPa}$; $T_2 = 3638 \text{ K}$.

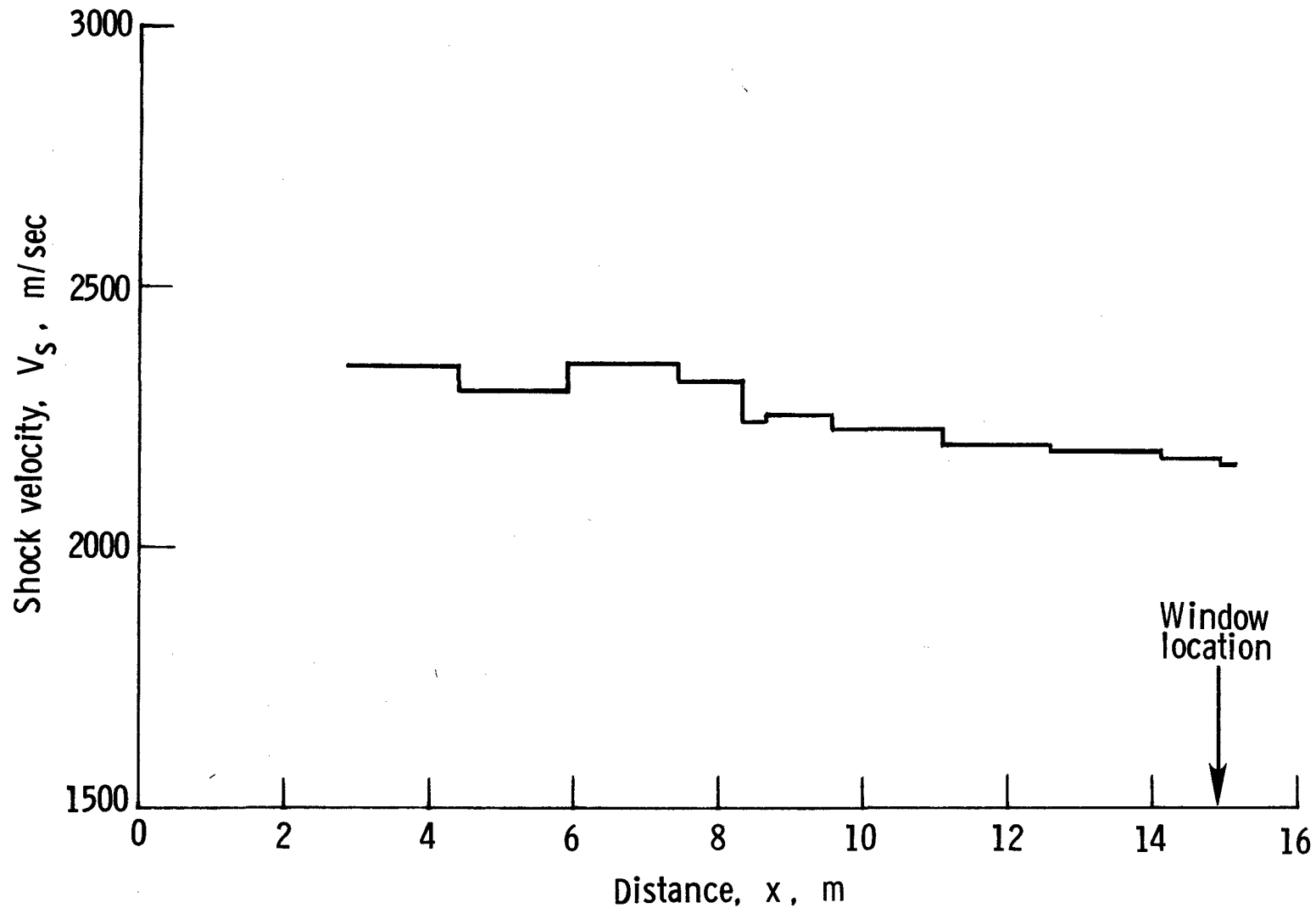
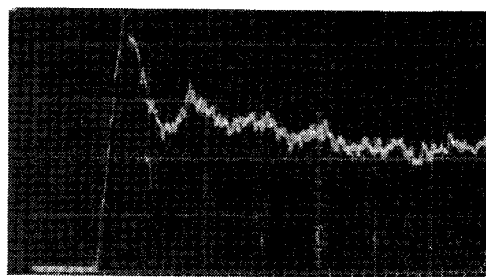
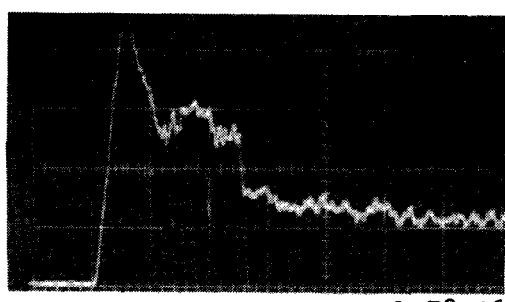


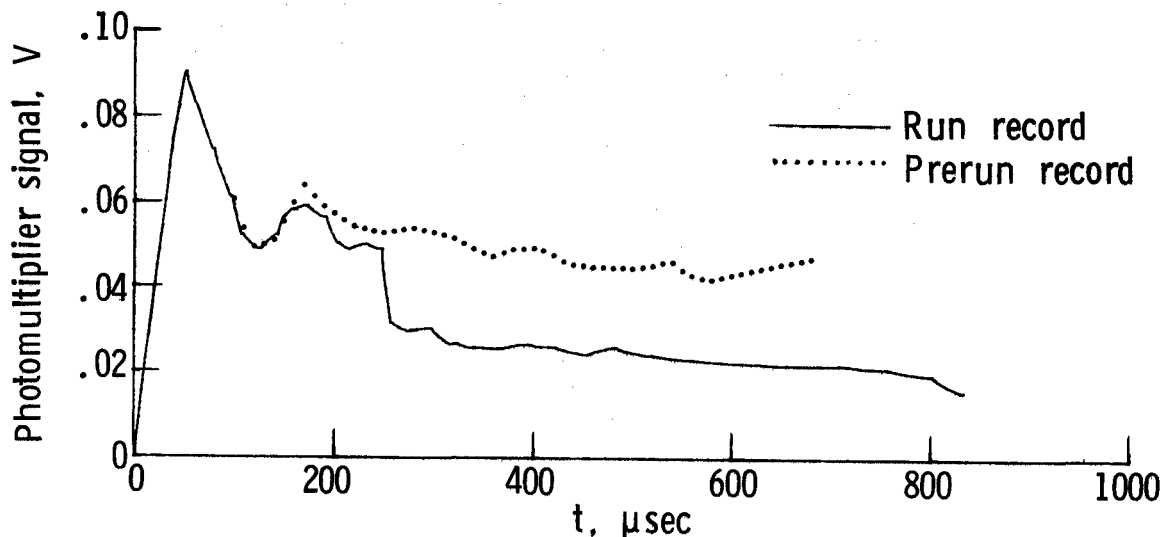
Figure 4.- Shock velocity as determined from time intervals between stations.



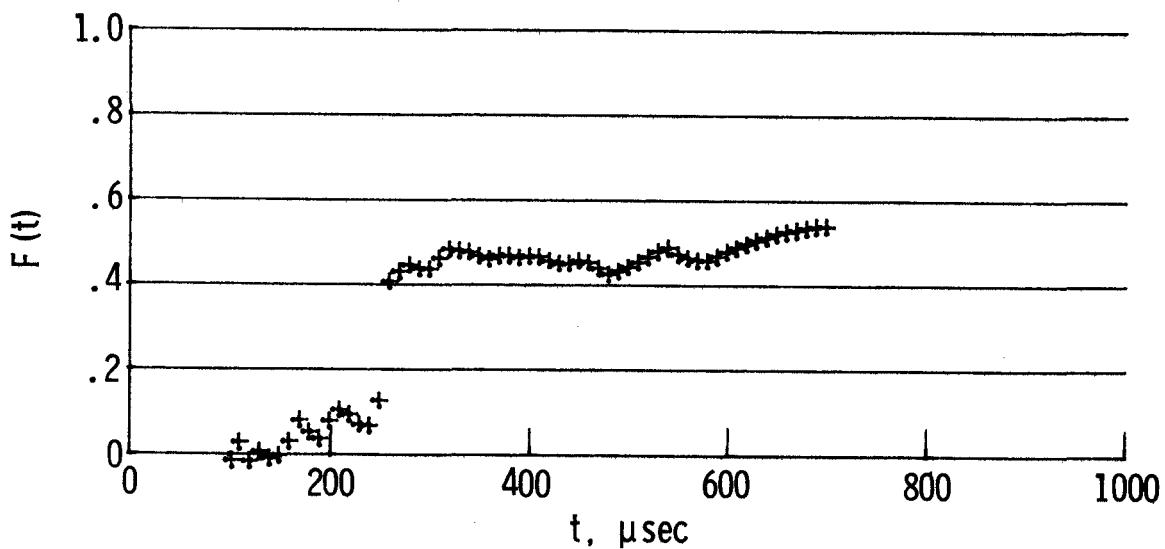
(a) Prerun light pulse.



(b) Light pulse during run.
L-78-16

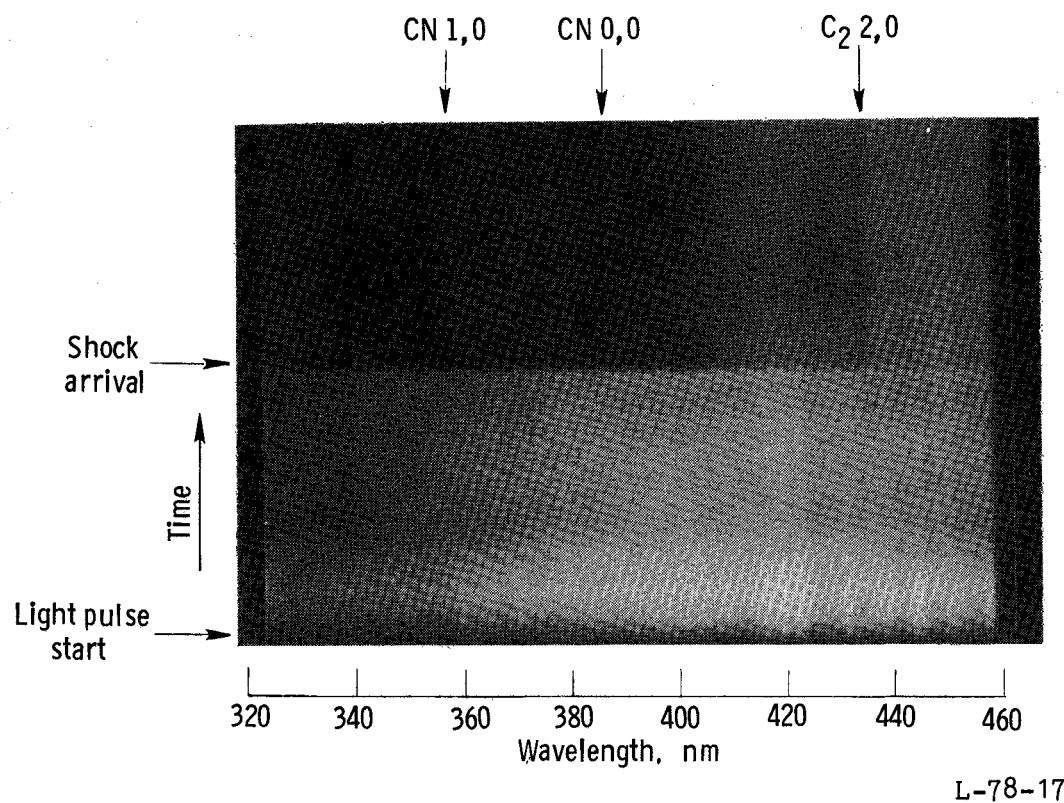


(c) Digitized records of run and prerun traces.



(d) Absorption parameter F(t).

Figure 5.- Sample spectrograph channel record and method of determining absorption parameter F(t). $p_{50} = 105$ kPa; $T_{50} = 3709$ K.



(a) Print of drum camera film.

L-78-17



(b) Microdensitometer tracings.

Figure 6.- Sample drum camera record and microdensitometer tracings.
 $p_{50} = 118 \text{ kPa}$; $T_{50} = 3686 \text{ K}$.

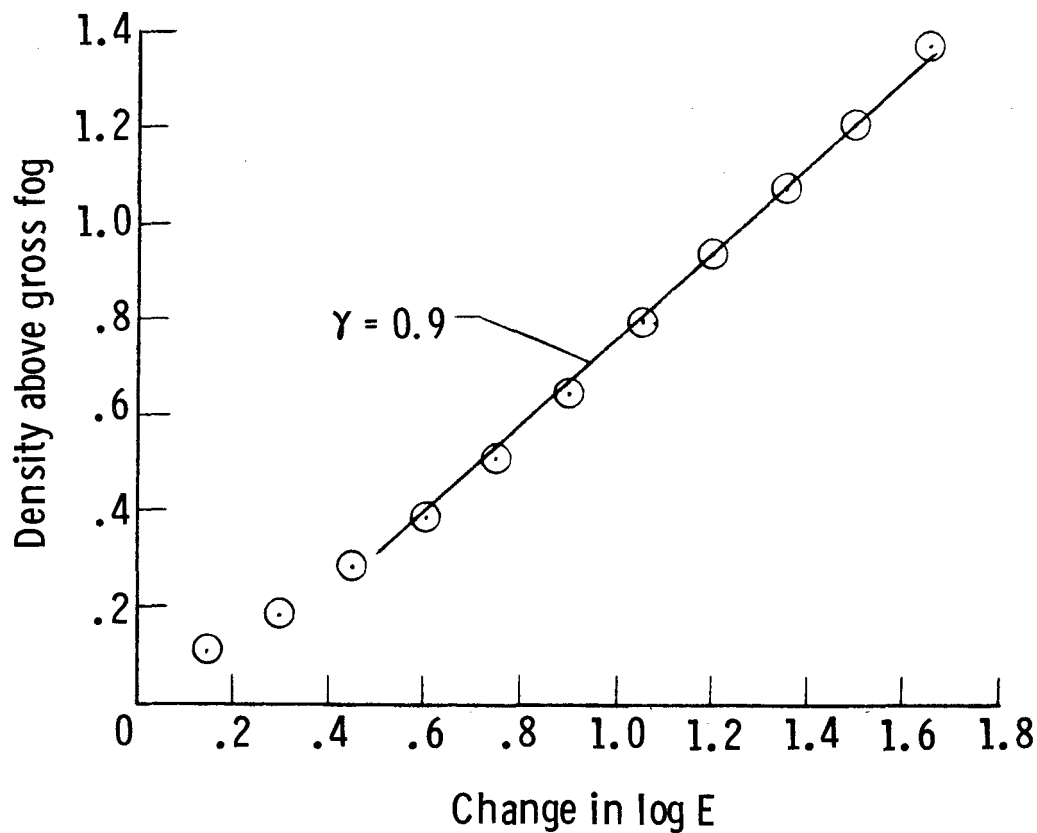


Figure 7.- Results of sensitometer calibration of film.

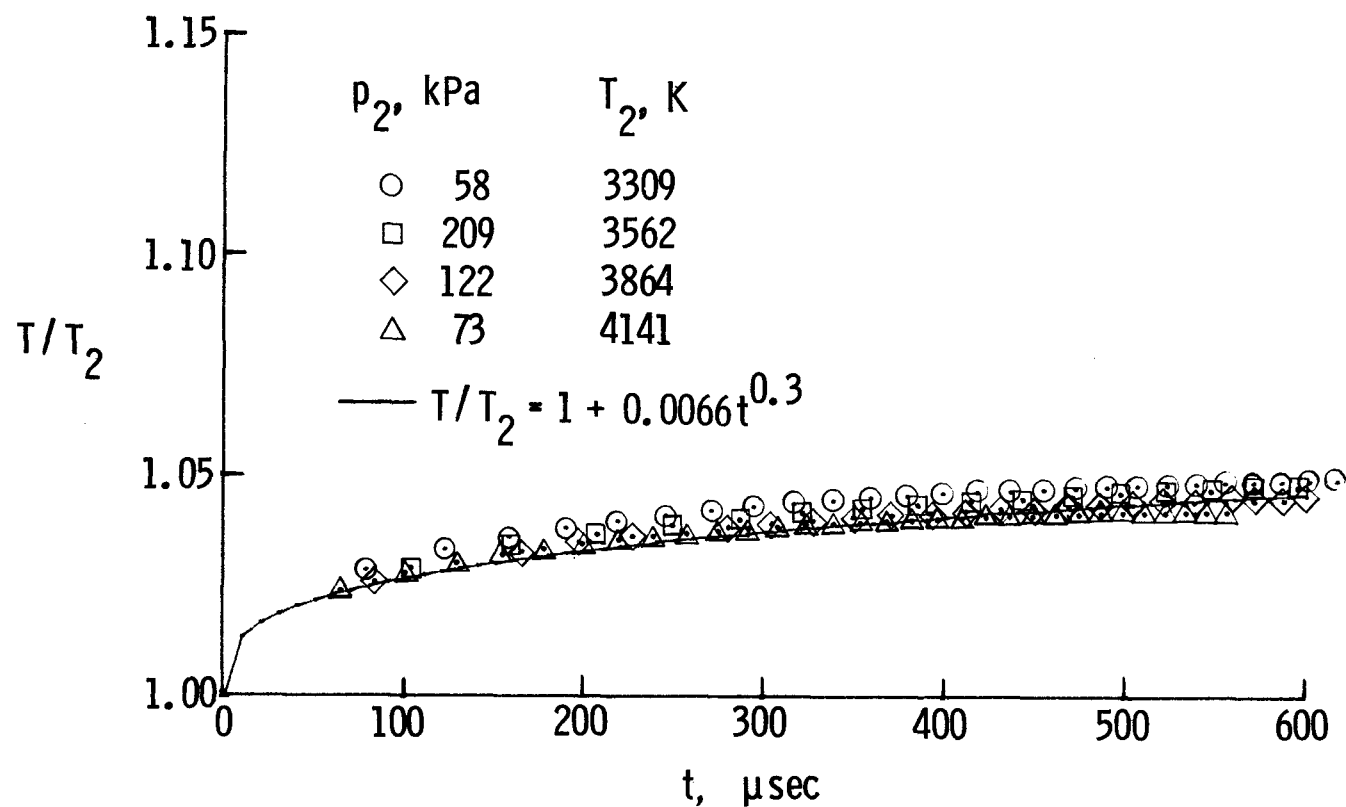


Figure 8.- Calculated temperature variation behind shock for various sample runs.

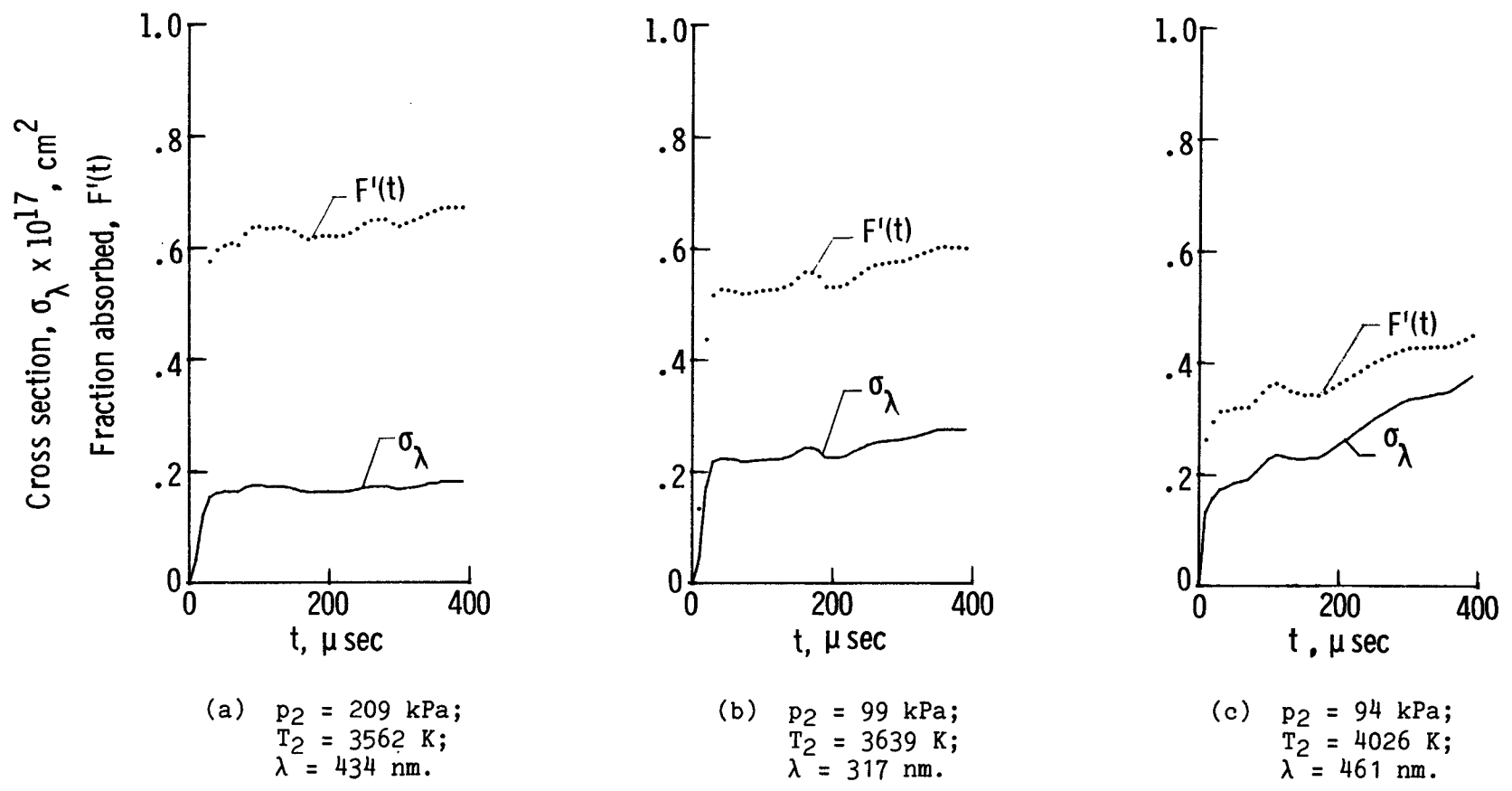


Figure 9.- Example of time variation of absorption $F(t)$ and resulting cross section σ_λ after correction for free-stream state variation.

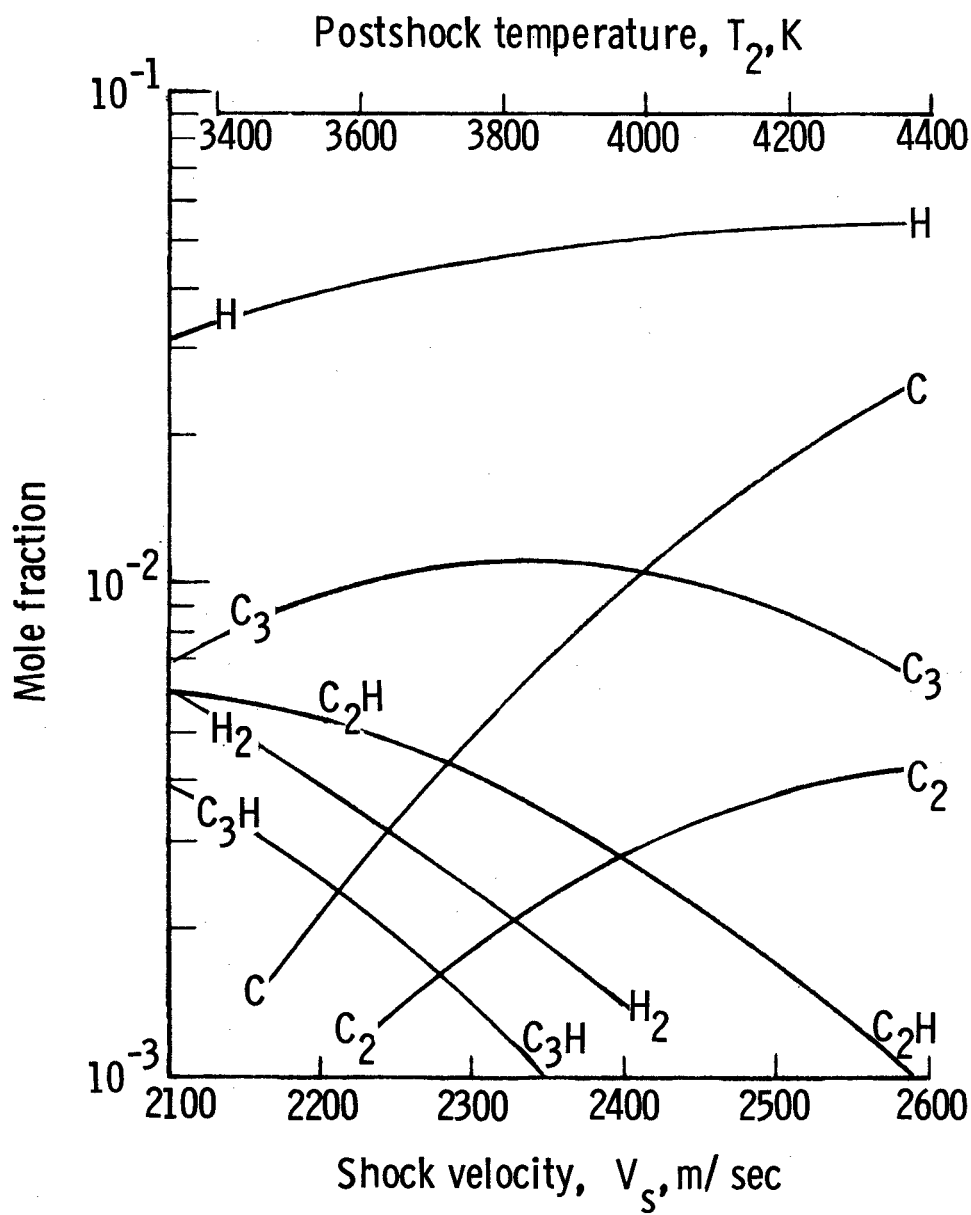


Figure 10.- Mole fractions of principal species behind a shock wave into a gas mixture of 97 percent argon, 3 percent C_2H_2 . $p_1 = 1.72$ kPa.
(Argon is not shown.)

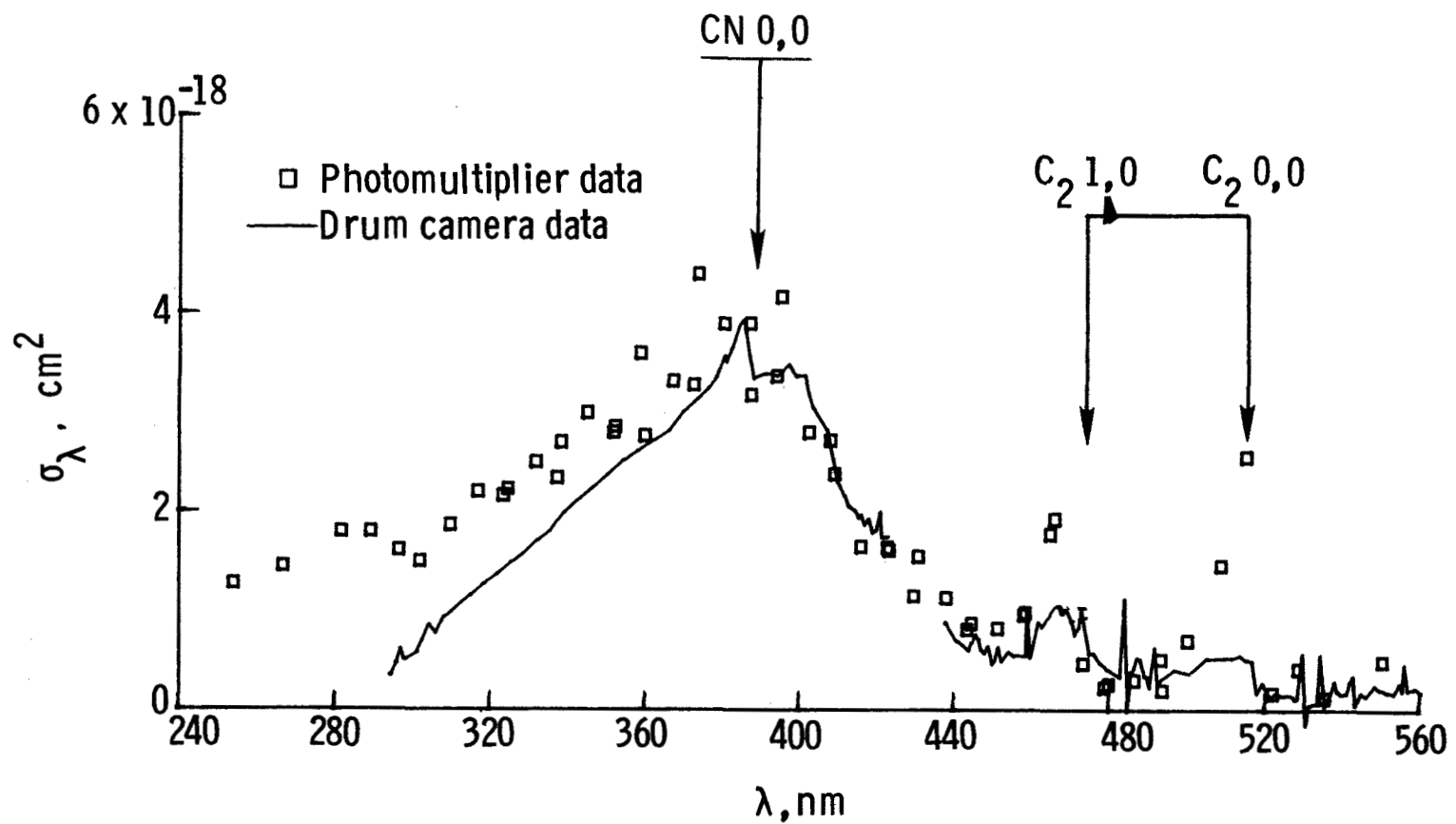


Figure 11.- Spectral survey of C_3 cross section at $T_{50} = 3723 \pm 47 \text{ K}$.

97

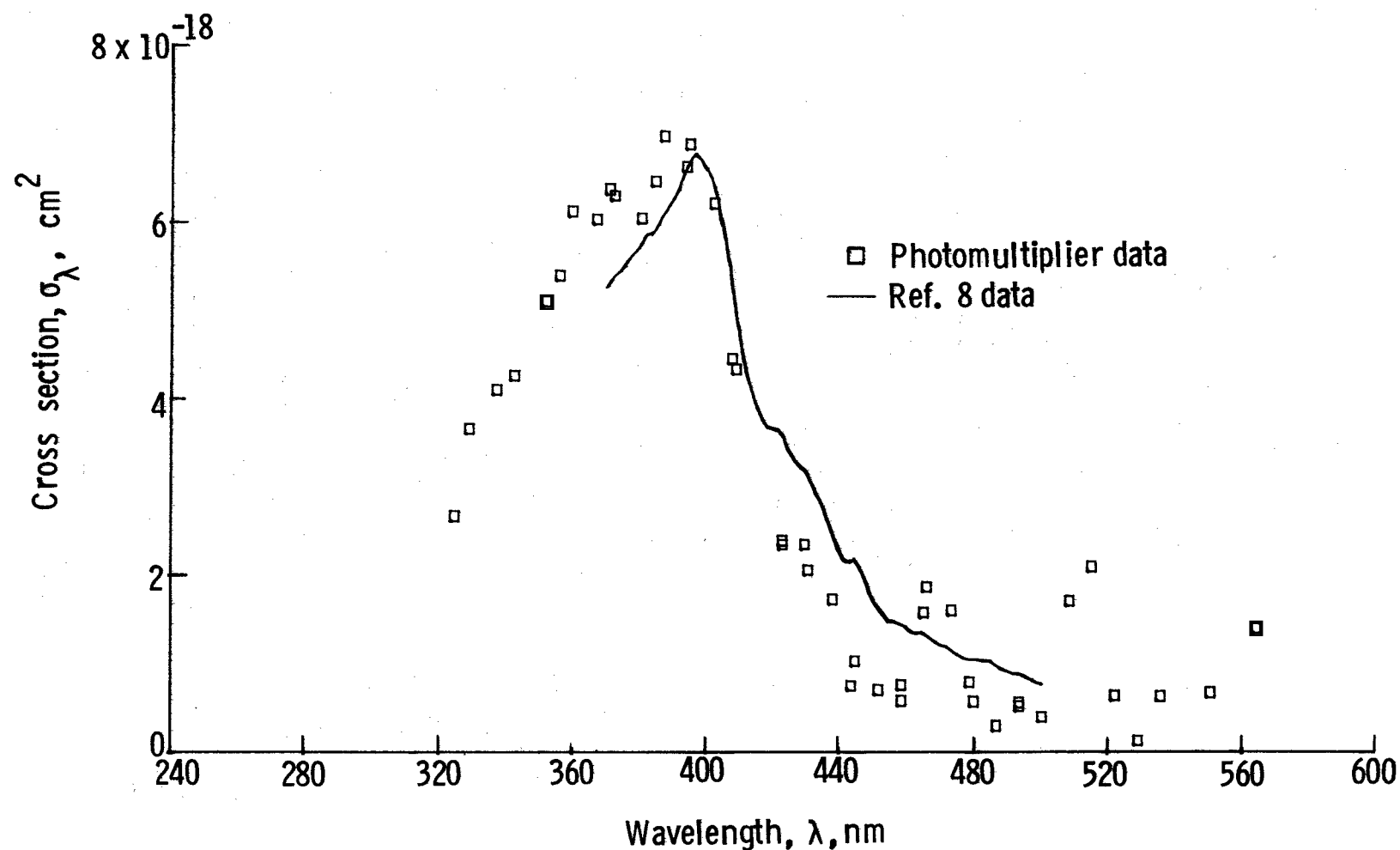
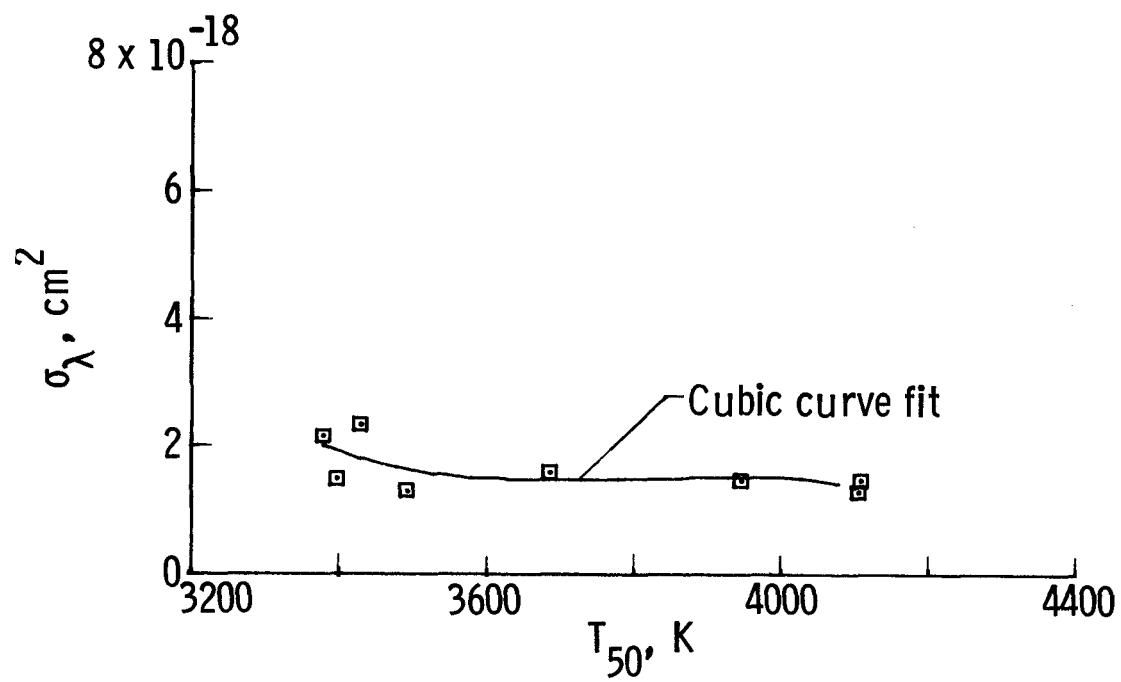
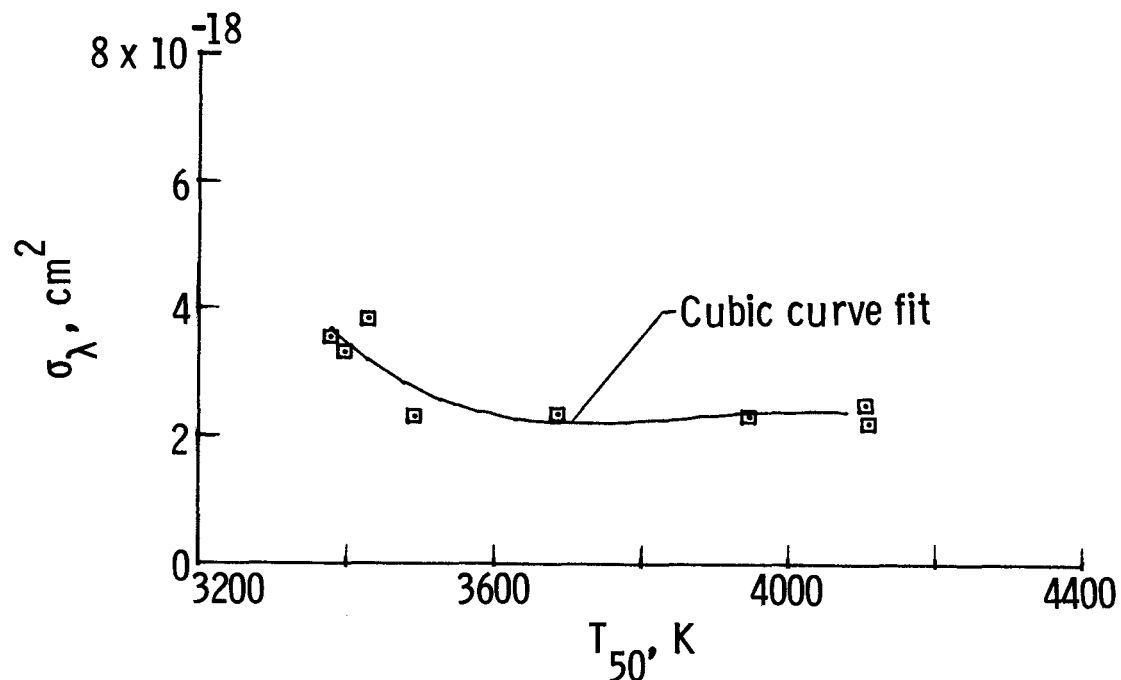


Figure 12.- Comparison of cross sections measured at $T_{50} = 3240 \pm 25$ K with those of reference 8 data at $T = 3200$ K.

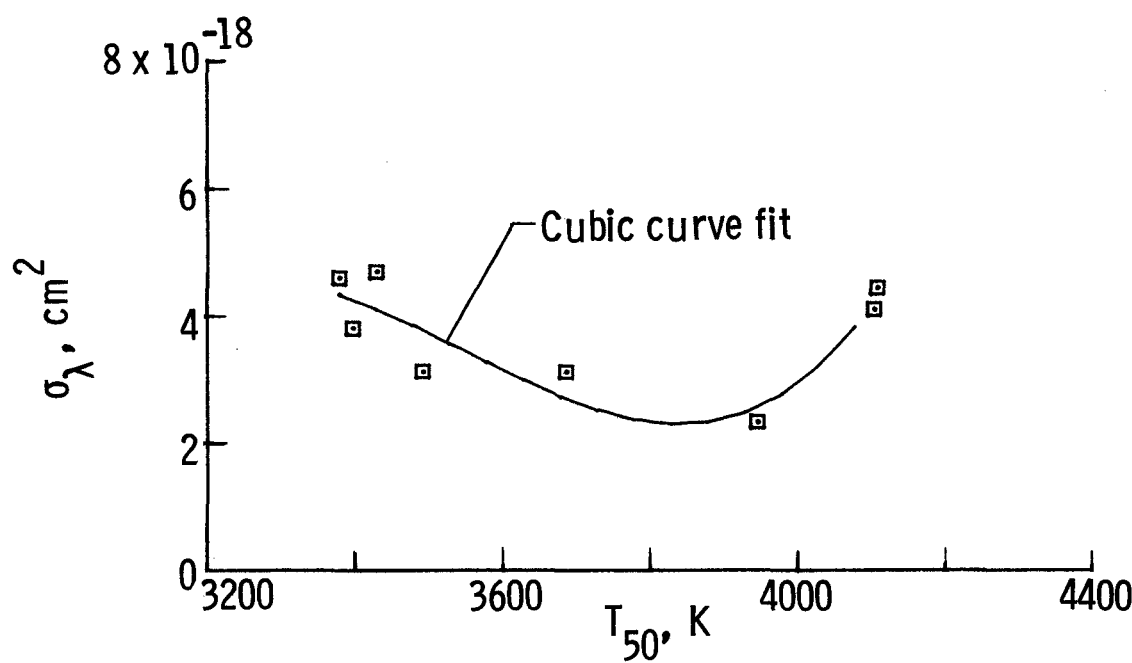


(a) $\lambda = 301 \text{ nm.}$

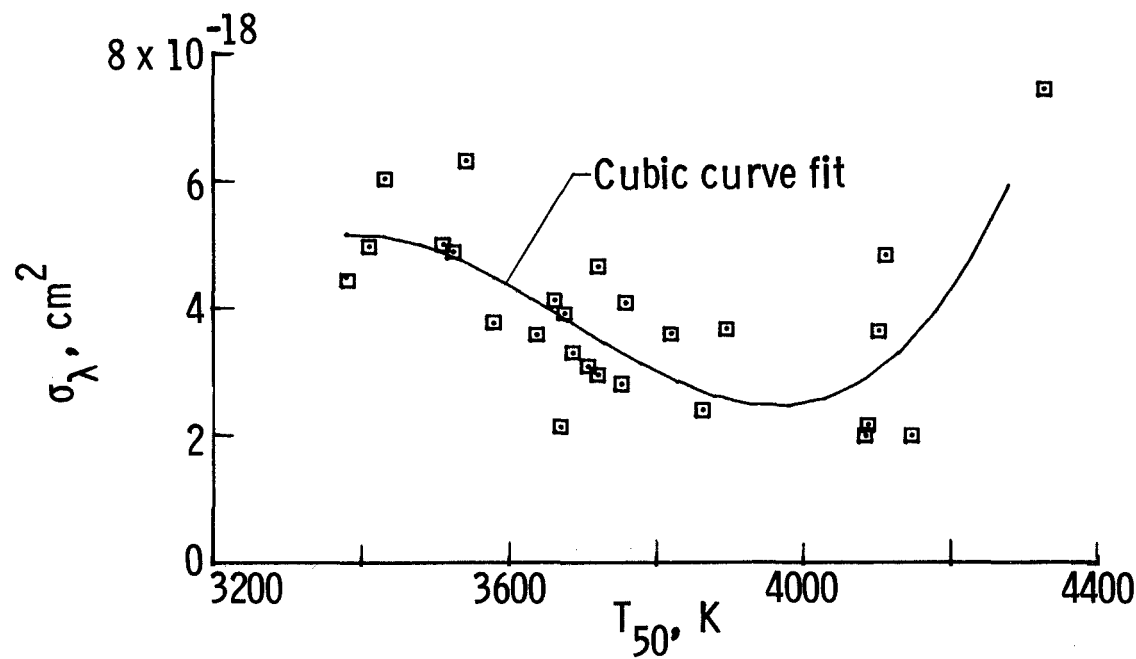


(b) $\lambda = 344 \text{ nm.}$

Figure 13.- Variation of absorption cross section with temperature for selected wavelengths.

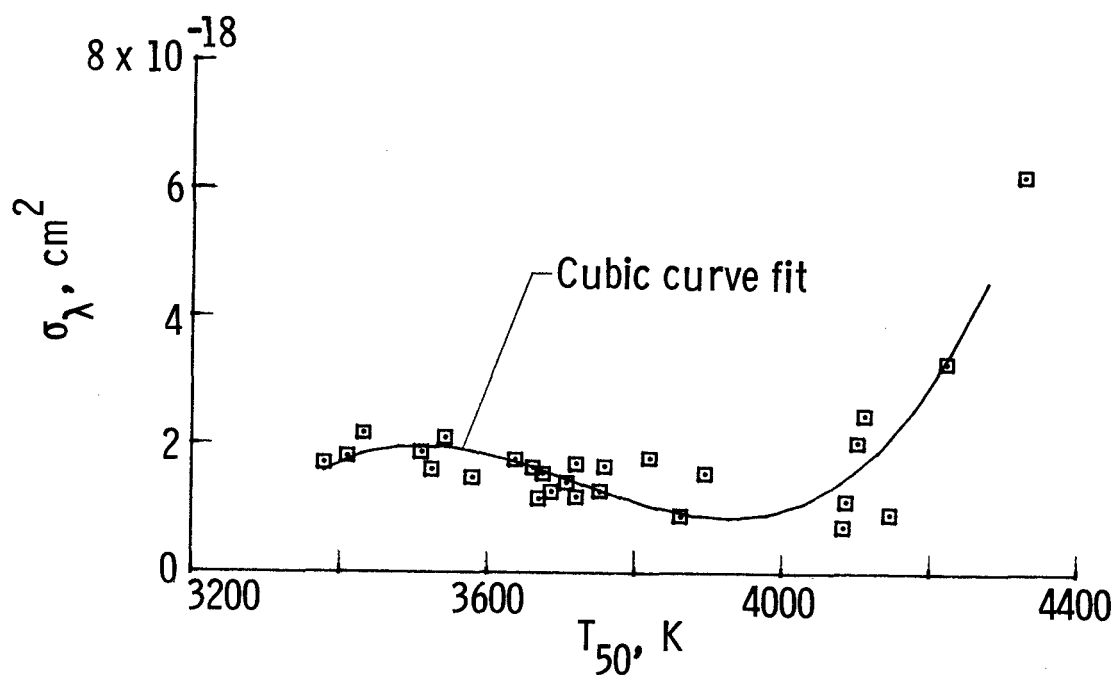


(c) $\lambda = 371 \text{ nm.}$

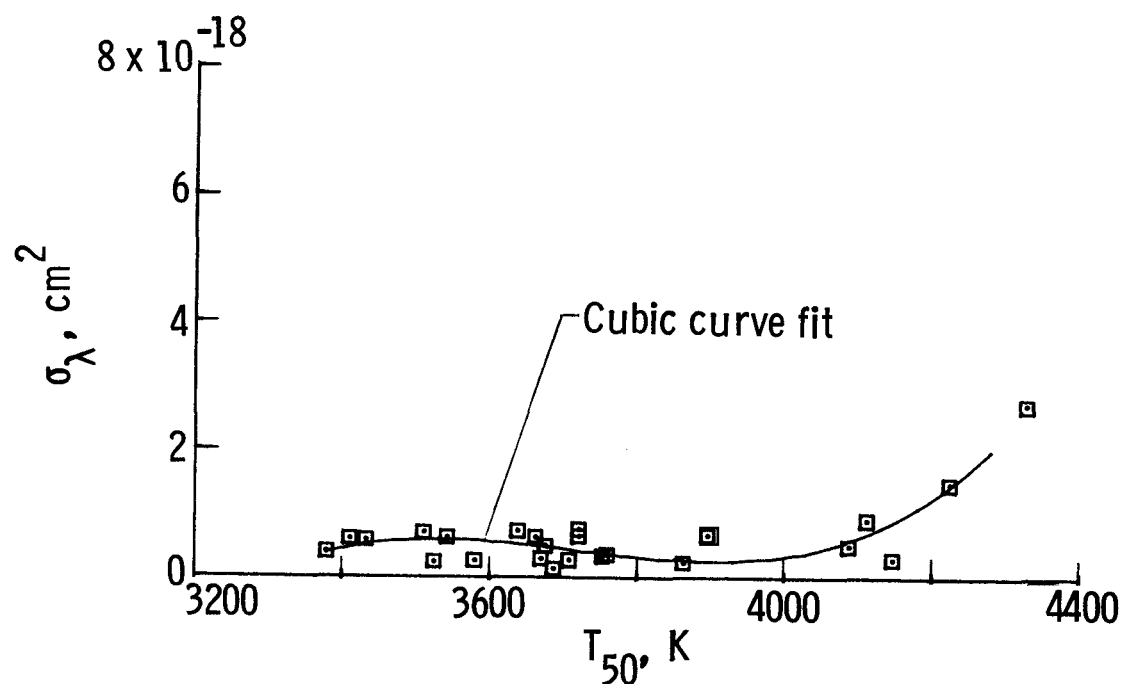


(d) $\lambda = 405 \text{ nm.}$

Figure 13.- Continued.

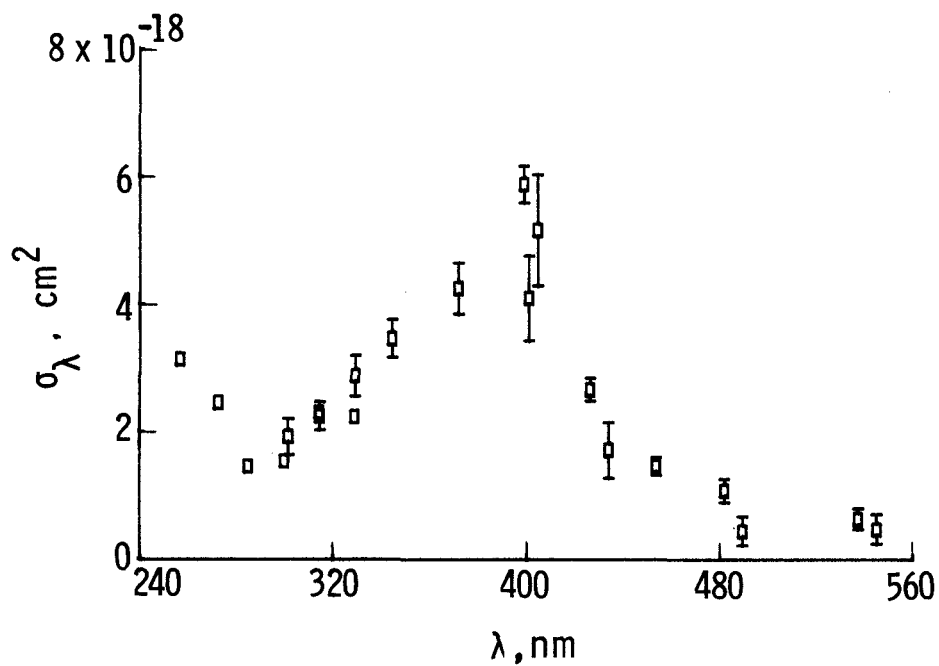


(e) $\lambda = 434 \text{ nm.}$

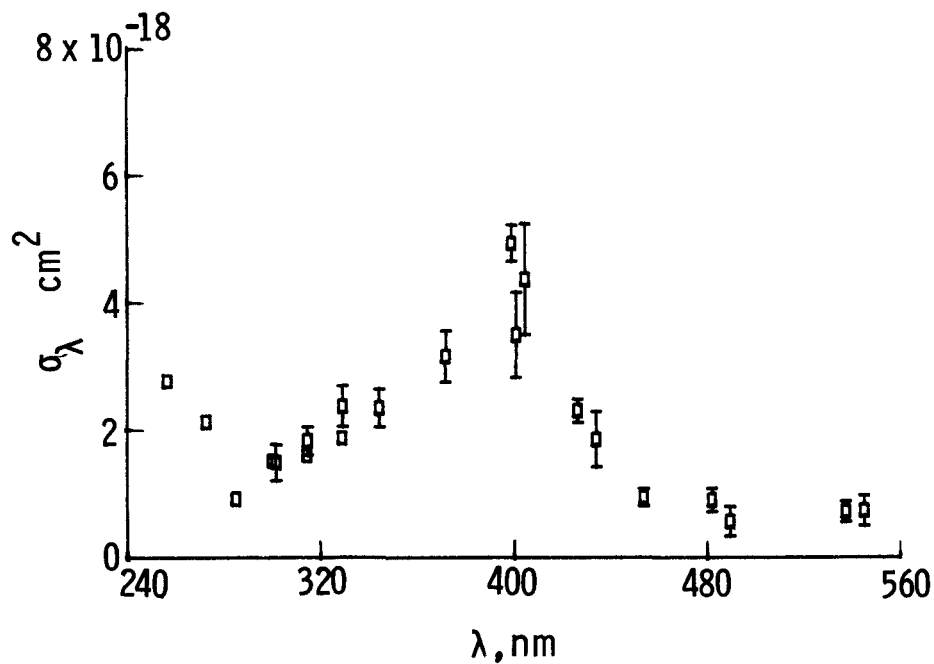


(f) $\lambda = 490 \text{ nm.}$

Figure 13.- Concluded.

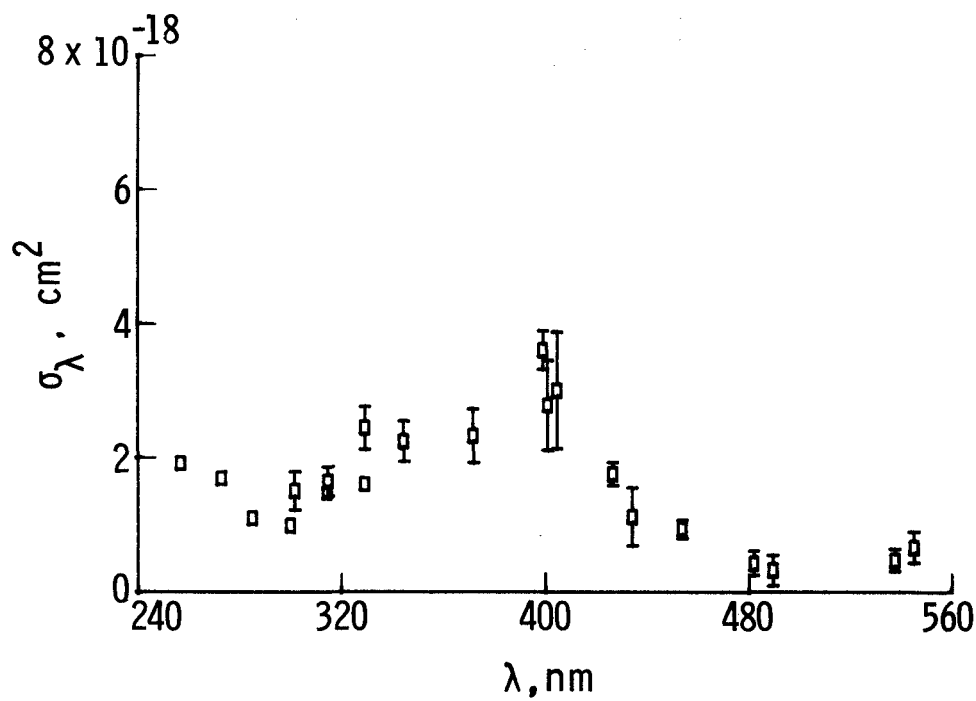


(a) $T = 3400 \text{ K.}$

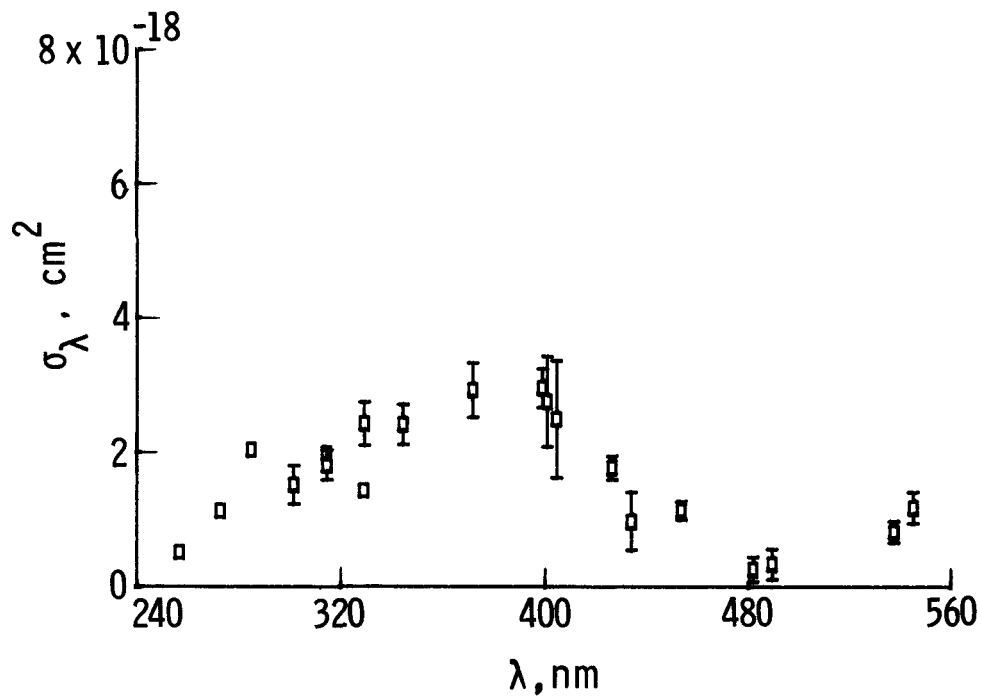


(b) $T = 3600 \text{ K.}$

Figure 14.- Spectral cross-section profile at selected temperatures.
Symbols are value of cubic curve fit; bars indicate standard deviation of data (where sufficient data available).



(c) $T = 3800 \text{ K.}$



(d) $T = 4000 \text{ K.}$

Figure 14.- Concluded.

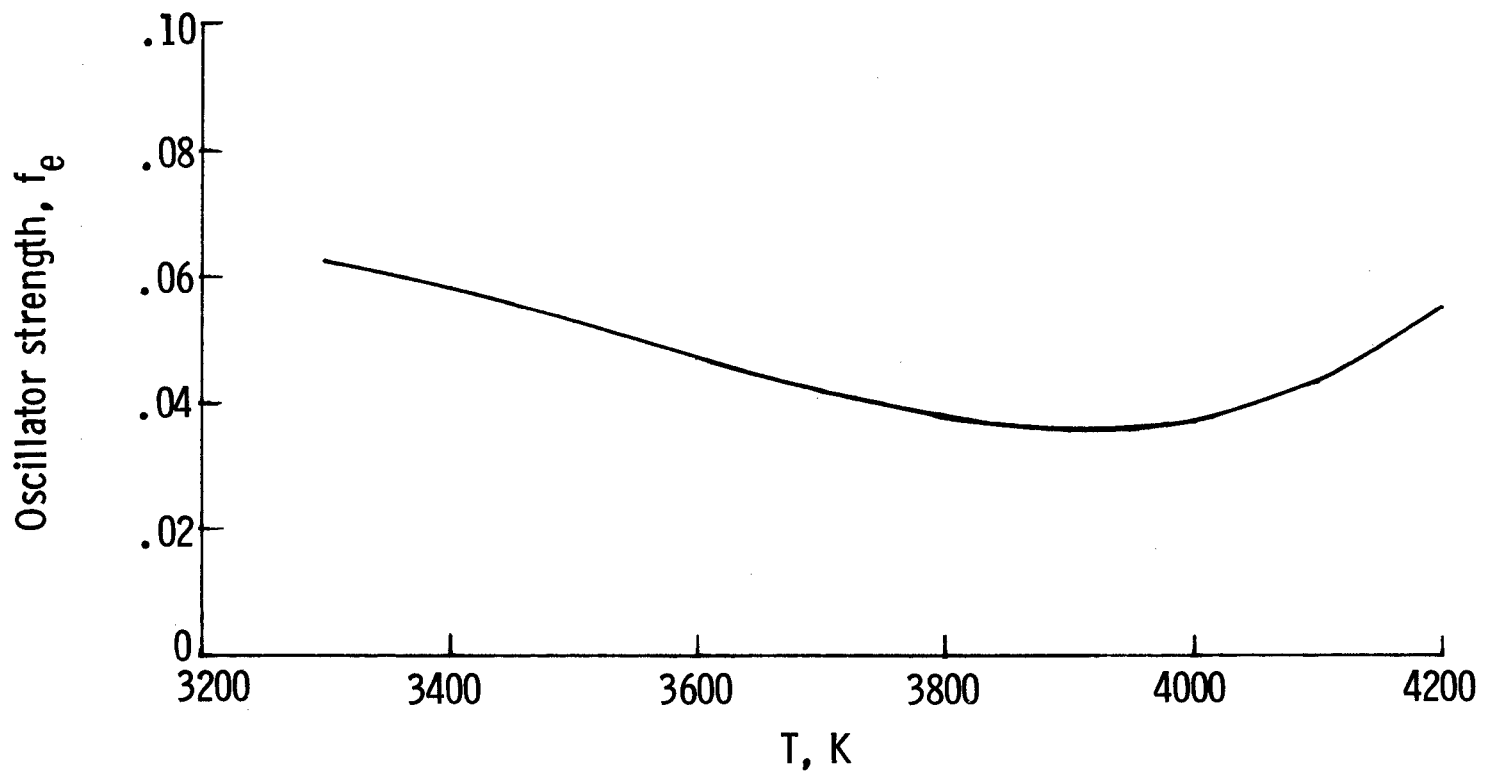


Figure 15.- Electronic oscillator strength calculated from present experiment
as a function of test-gas temperature.

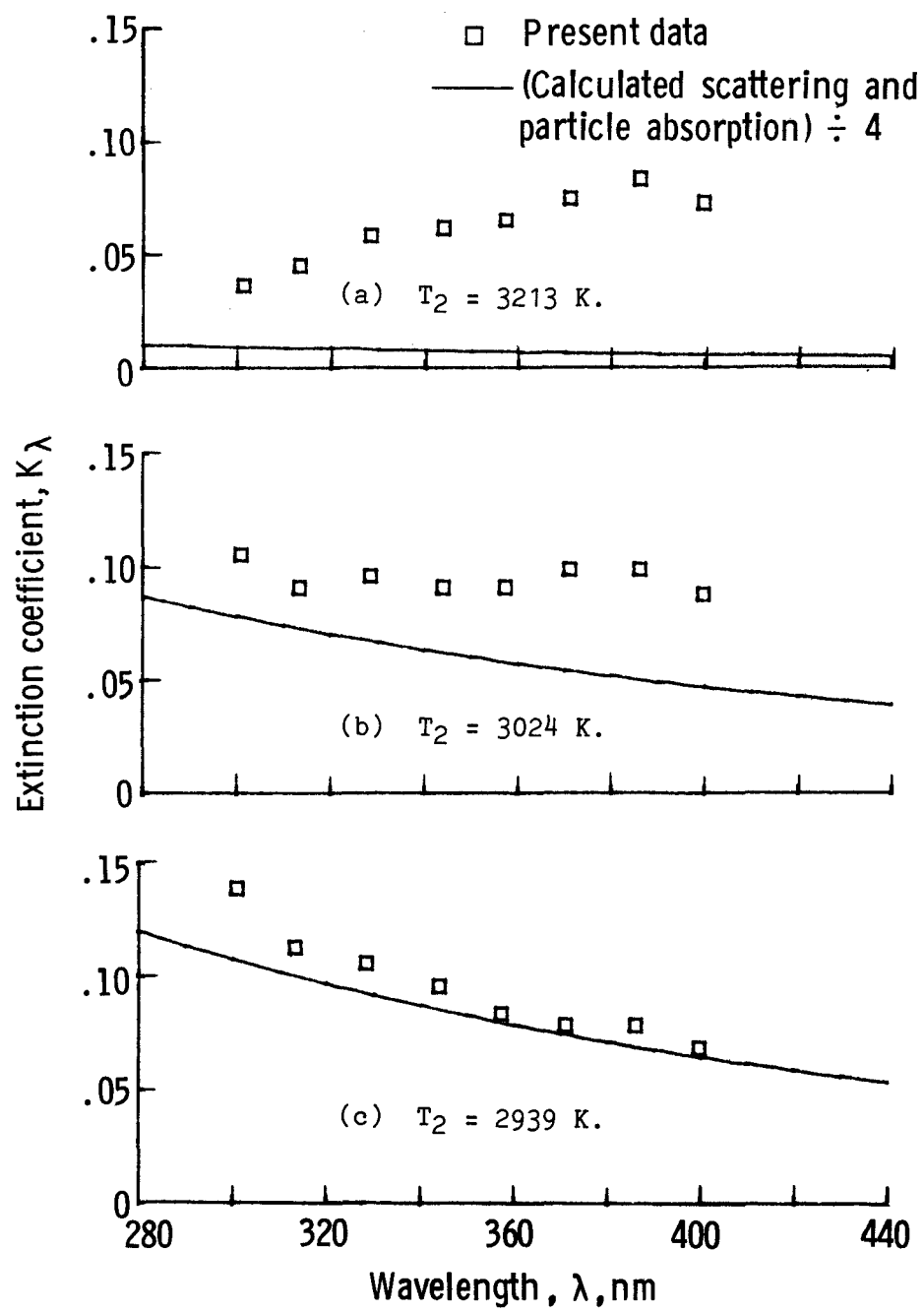
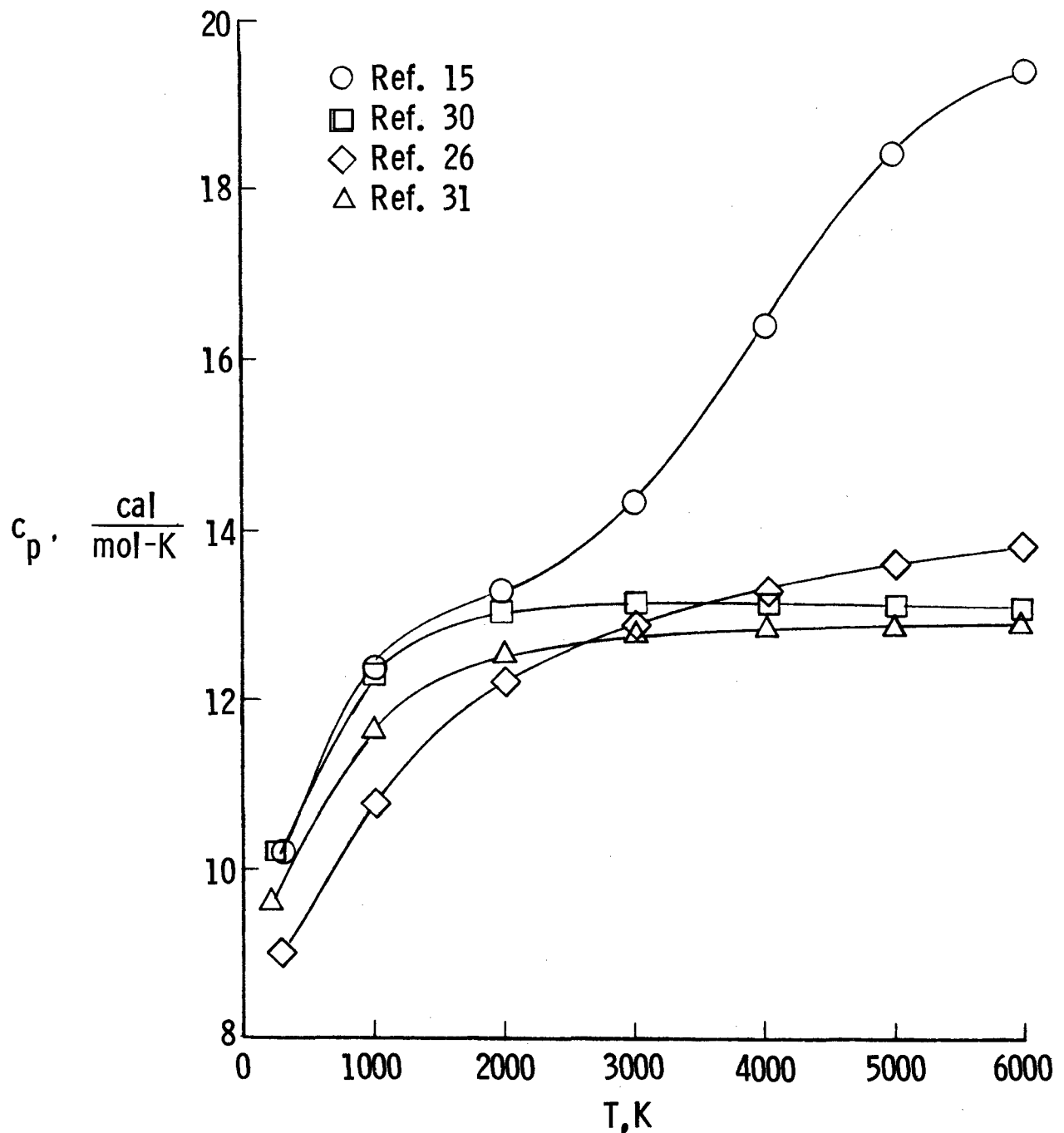
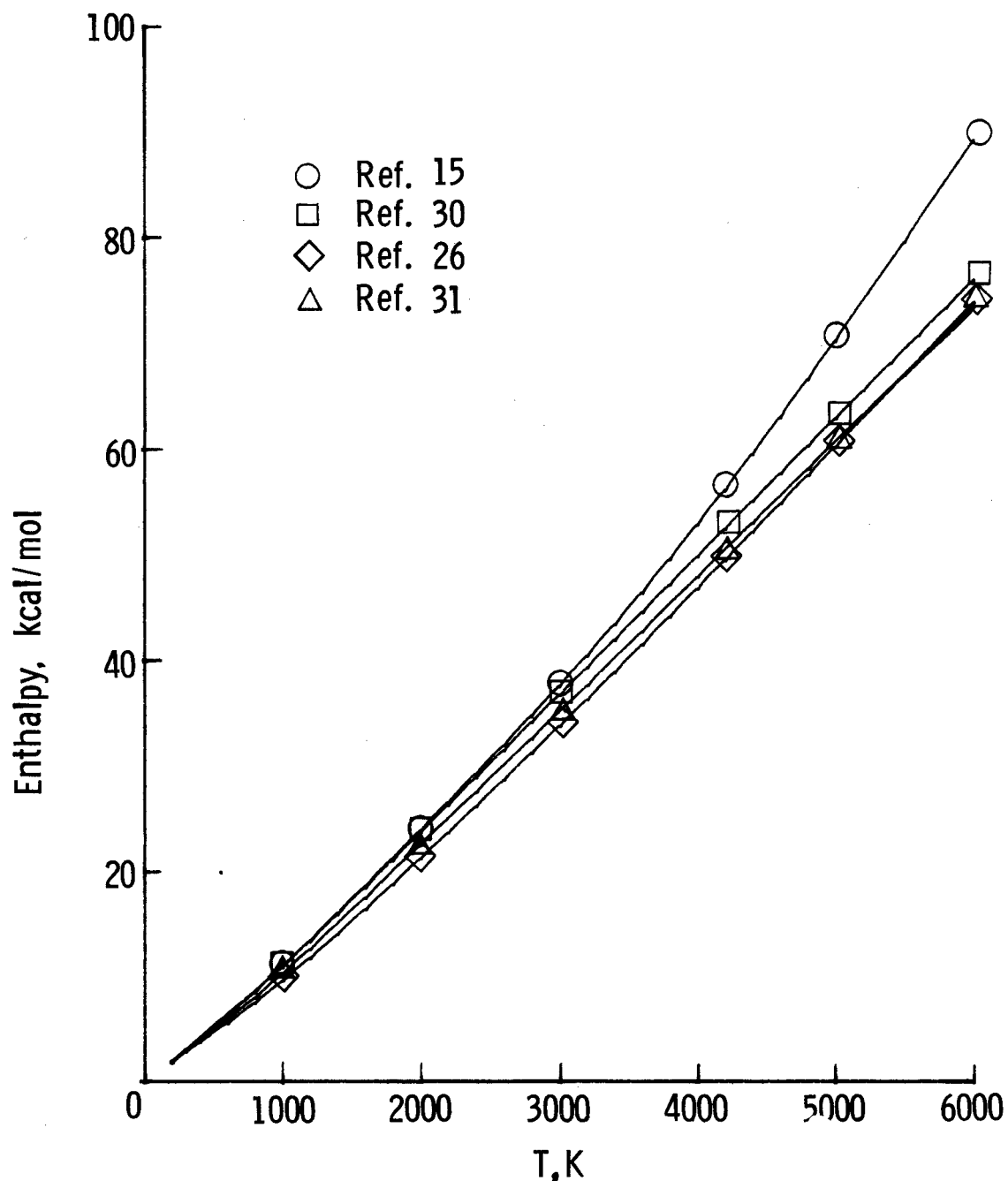


Figure 16.- Measured extinction coefficient at various temperatures compared with calculated extinction due to scattering and absorption of 30-nm-radius particles.



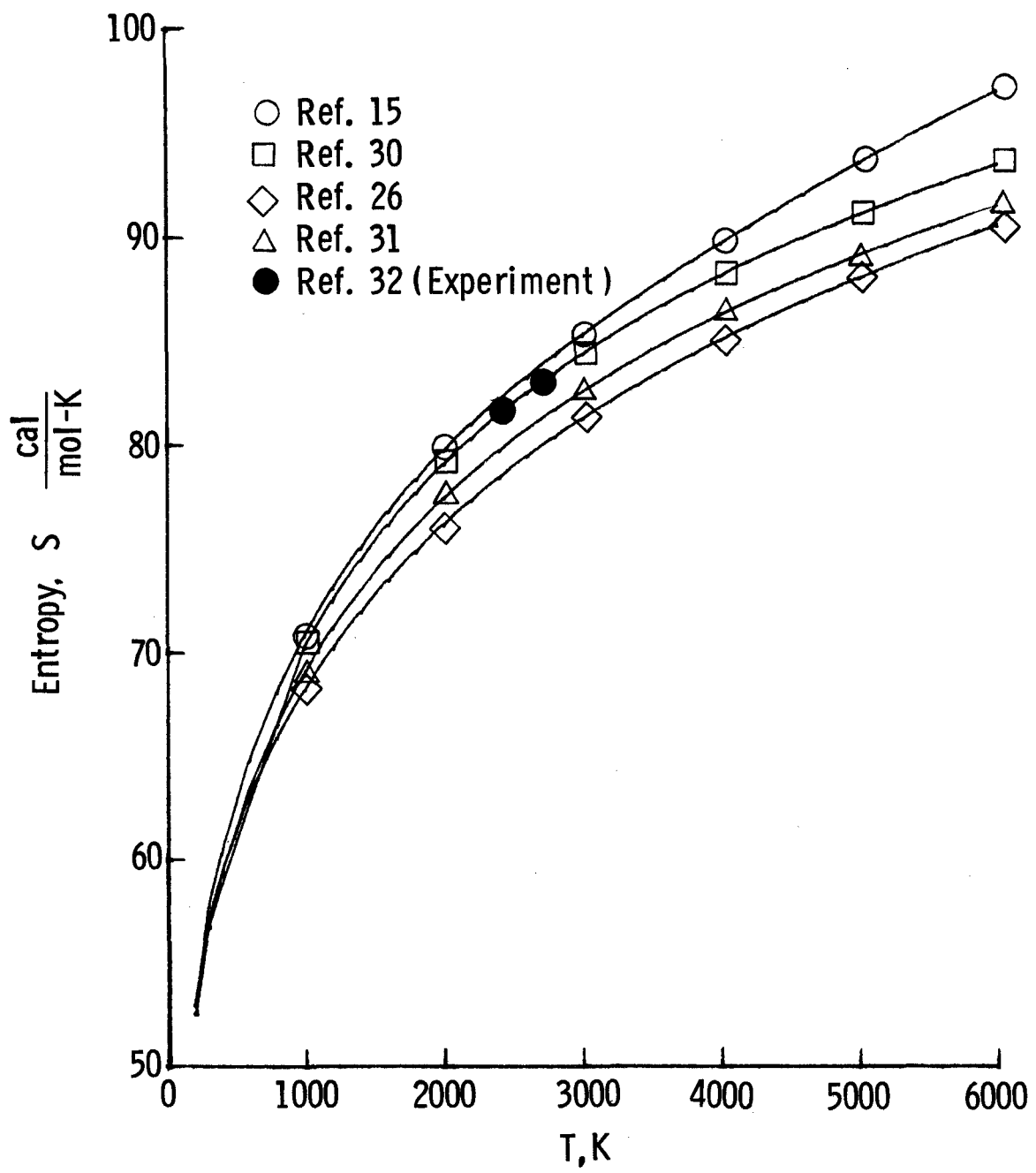
(a) Specific heat at constant pressure.

Figure 17.- Comparison of thermal properties of C_3
as calculated by four methods.



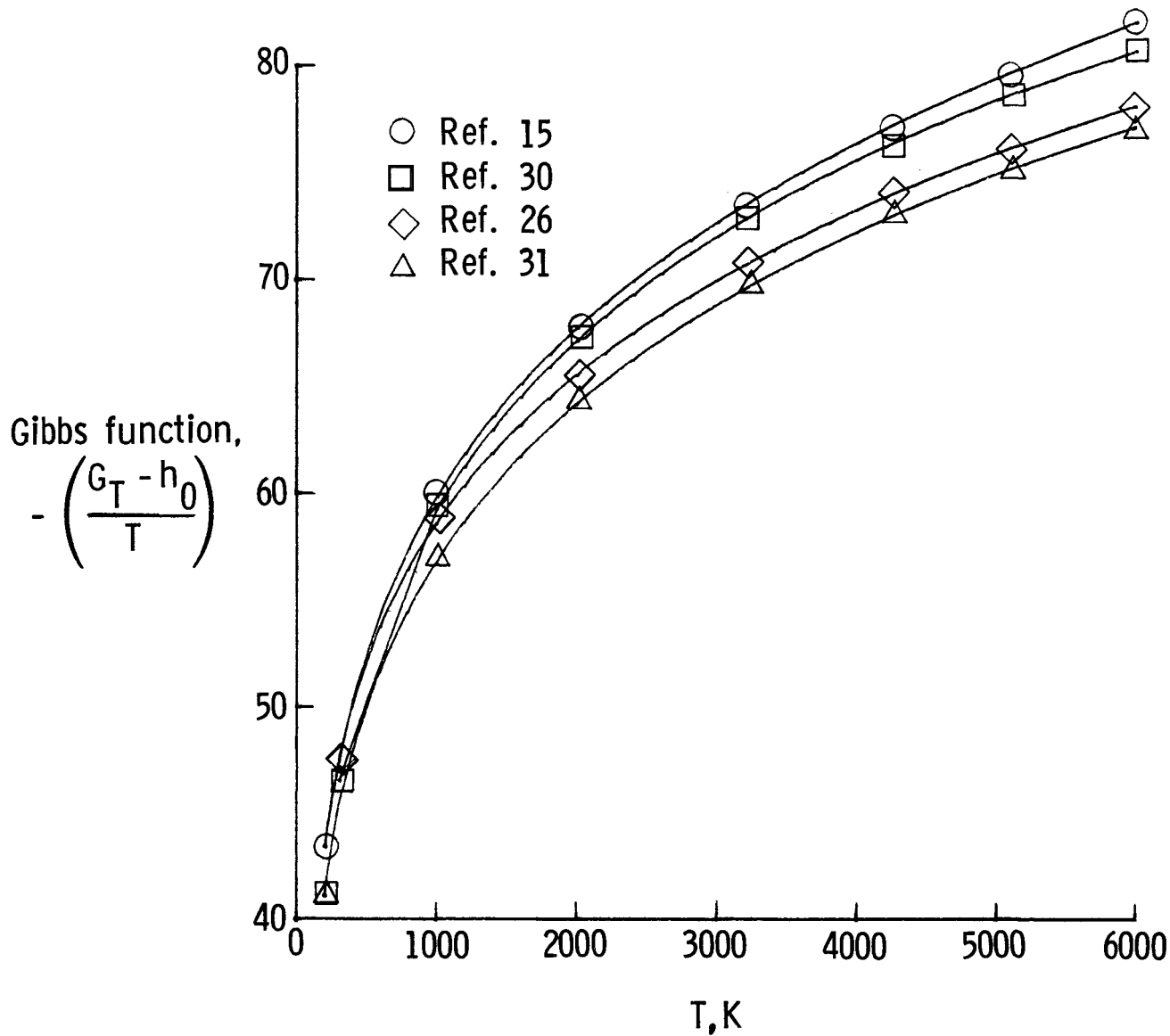
(b) Enthalpy.

Figure 17.- Continued.



(c) Entropy.

Figure 17.- Continued.



(d) Gibbs function.

Figure 17.- Concluded.

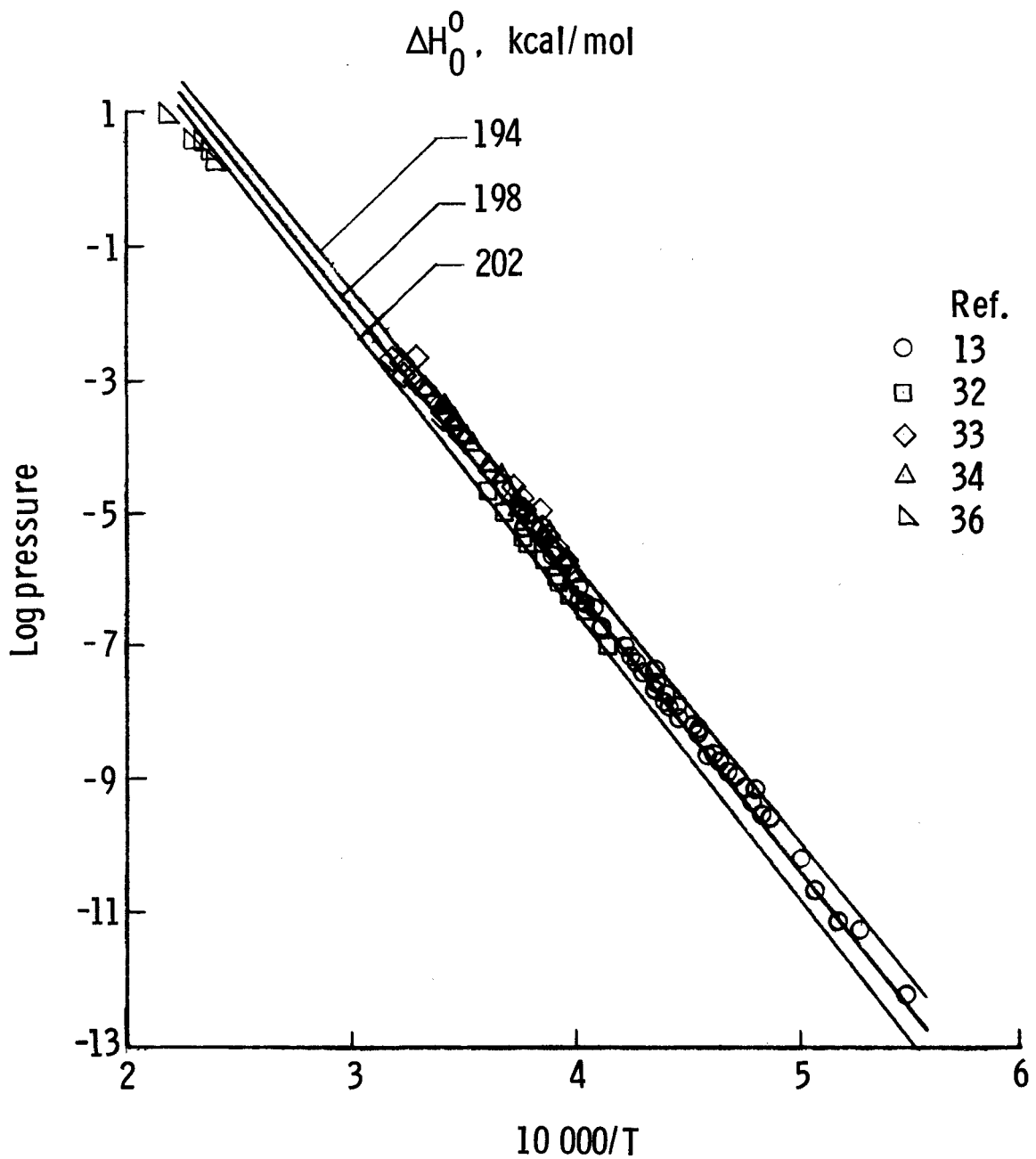


Figure 18.- Summary of C_3 vapor-pressure data.

1. Report No. NASA TP-1141	2. Government Accession No.	3. Recipient's Catalog No.	
4. Title and Subtitle THE OPTICAL ABSORPTION OF TRIATOMIC CARBON C ₃ FOR THE WAVELENGTH RANGE 260 TO 560 nm		5. Report Date March 1978	
		6. Performing Organization Code	
7. Author(s) Jim J. Jones		8. Performing Organization Report No. L-11871	
9. Performing Organization Name and Address NASA Langley Research Center Hampton, VA 23665		10. Work Unit No. 506-26-20-01	
		11. Contract or Grant No.	
12. Sponsoring Agency Name and Address National Aeronautics and Space Administration Washington, DC 20546		13. Type of Report and Period Covered Technical Paper	
		14. Sponsoring Agency Code	
15. Supplementary Notes			
16. Abstract <p>The spectral absorption properties of C₃ have been measured in a shock tube containing a test-gas mixture of acetylene diluted with argon. The absorption of a pulsed xenon light source was measured by means of eight photomultiplier channels to a spectrograph and an accompanying drum camera. The postshock test-gas temperature and pressure were varied over the ranges 3240 to 4300 K and 37 to 229 kPa, respectively.</p> <p>The results showed appreciable absorption by C₃ for the wavelength range 300 to 540 nm. The various reported measurements of the heat of formation of C₃ which are available in the open literature have been reviewed, and a value of 198 kcal/mol is recommended. This value, along with best available values for other species, was used to calculate the number density of C₃ for the conditions of the present experiments in order to compute absorption cross section or electronic oscillator strength. The computed electronic oscillator strength varied from a high of 0.062 at 3300 K to a low of 0.036 at 3900 K.</p>			
17. Key Words (Suggested by Author(s)) Triatomic carbon Spectral absorption cross section Radiative heat transfer Carbon vapor		18. Distribution Statement Unclassified - Unlimited Subject Category 72	
19. Security Classif. (of this report) Unclassified	20. Security Classif. (of this page) Unclassified	21. No. of Pages 58	22. Price* \$5.25

* For sale by the National Technical Information Service, Springfield, Virginia 22161

NASA-Langley, 1978



9 11U,H, 022778 S00903DS
DEPT OF THE AIR FORCE
AF WEAPONS LABORATORY
ATTN: TECHNICAL LIBRARY (SUL)
KIRTLAND AFB NM 87117

NASA
